INSTITUTO TECNOLÓGICO DE AERONÁUTICA

Élvis Falcão de Araújo

PERFORMANCE AND FINANCIAL ANALYSIS OF SOLAR PHOTOVOLTAIC SYSTEMS

Final Paper
2015

Course of Aeronautical Mechanical Engineering

CDU 621.383.5

Élvis Falcão de Araújo

PERFORMANCE AND FINANCIAL ANALYSIS OF SOLAR PHOTOVOLTAIC SYSTEMS

Advisor

Prof. João Batista do Porto Neves Júnior (ITA)

AERONAUTICAL MECHANICAL ENGINEERING

São José dos Campos
Instituto Tecnológico de Aeronáutica

2015

Cataloging-in Publication Data
Documentation and Information Division

de Araújo, Élvis Falcão
Performance and Financial Analysis of Solar Photovoltaic Systems / Élvis Falcão de Araújo.
São José dos Campos, 2015.
85f.

Final paper (Undergraduation study) – Course of Aeronautical Mechanical Engineering–
Instituto Tecnológico de Aeronáutica, 2015. Advisor: Prof. João Batista do Porto Neves Júnior.

1. Costs. 2. Energy. 3. Photovoltaics. I. Instituto Tecnológico de Aeronáutica. II. Title.

BIBLIOGRAPHIC REFERENCE

DE ARAÚJO, Élvis Falcão. **Performance and Financial Analysis of Solar Photovoltaic Systems**. 2015. 85f. Final paper (Undergraduation study) – Instituto Tecnológico de Aeronáutica, São José dos Campos.

CESSION OF RIGHTS

AUTHOR'S NAME: Élvis Falcão de Araújo
PUBLICATION TITLE: Performance and Financial Analysis of Solar Photovoltaic Systems.
PUBLICATION KIND/YEAR: Final paper (Undergraduation study) / 2015

Élvis

Élvis Falcão de Araújo
H8B Street, 221
12228-461 – São José dos Campos–SP

PERFORMANCE AND FINANCIAL ANALYSIS OF SOLAR PHOTOVOLTAIC SYSTEMS

This publication was accepted like Final Work of Undergraduation Study

Élvis Falcão de Araújo
Author

João Batista do Porto Neves Júnior (ITA)
Advisor

Prof. Dr. Jesuíno Takachi Tomita
Course Coordinator of Aeronautical Mechanical Engineering

São José dos Campos: NOVEMBER 18, 2015.

To friends, family and people who fought for justice and peace all around the World: Malcon X, Gandhi, Bob Marley, Zumbi dos Palmares, Antônio Conselheiro, Tupac Shakur, Martin Luther King, Jesus Christ.

Acknowledgments

I would like to thank my family, for supporting me all days of my life, my friends for sharing moments of happiness and struggle, and my professors, for building in me the knowledge necessary to achieve one more goal. I would like to thank all the gangsta rap singers in the World as well, for songs that gave me motivation to fight for my dreams, and more important, thank God for making everything worth it.

"Wars come and go,
but my soldiers stay eternal."
— TUPAC SHAKUR

Abstract

This work is a performance and financial analysis of different designs for photovoltaic solar panel arrays to be installed in an Automated Transit Network prototype with the objective of supplying the necessary electricity to make it work properly. An Automated Transit Network is a personal transportation system that moves following guideways and works automatically, with no driver, going directly to the station chosen by the rider without stop. The prototype is a project of San Jose State University called Spartan Superway and consists of a suspended cabin moving under a guideway. The designed systems would be installed above the tracks.

An electrical photovoltaic system is consisted of solar modules arrays connected in parallel or in series attached to a Maximum Power Point Tracker that controls the operation point (voltage and current) to optimize power output. This is linked to a DC load, or a battery, or an inverter that produces AC power to be input into an AC Load or into the grid.

The analysis for each design considered data about the local weather to calculate annual irradiance, wind speed and temperature, performance characteristics of modules and inverters used in the system, possible losses caused by shading, snow, mismatch, diodes and connections, DC wiring, nameplate, DC optimizer, AC wiring or step-up transformer, lifetime degradation, battery configurations, system costs, financial parameters, federal and state incentives, electricity rates and electric load. The results include a monthly evaluation of cash flow and energy production and a list of financial and performance parameters of the photovoltaic systems.

List of Figures

List of Tables

List of Abbreviations and Acronyms

PV	Photovoltaic
MPPT	Maximum Power Point Tracking
ATN	Automated Transit Network
SAM	System Advisor Model
PPA	Power Purchase Agreement
TMY3	Typical Meteorological Year Version 3
NREL	National Renewable Energy Laboratory
STC	Standard Test Conditions
CEC	California Energy Comission
NMC	Nickel Manganese Cobalt Oxide
WACC	Weighted Average Cost of Capital
DSIRE	Database of State Incentives for Renewables and Efficiency
LCOE	Levelized Cost of Energy

List of Symbols

h	Plank's constant
E_p	Energy contained in a photon
ν	Wave frequency
λ	Wave length
I_L	Current generated by radiation
I_D	Saturation current of the diode
I	Current generated in the terminals
I_{ft}	Leakage current to ground
R_P	Parallel Resistance
R_S	Series Resistance
A	Curve correction parameter
V_{oc}	Open Circuit Voltage
I_{sc}	Short Circuit Current
$\dot{m}$	Mass flow rate
C_p	Specific heat
η_c	Instantaneous efficiency of the collector
I_c	Local irradiance
A_c	Collector area
I_g	Global irradiance
I_d	Diffuse irradiance
N_c	Total Nameplate Capacity in DC kW
C_i	Total Inverter Nameplate Capacity in AC kW
M_{mp}	Module Maximum Power in Wdc
A_t	Total module area
n_m	Number of inverters
V_{soc}	String open circuit voltage
V_{mp}	Maximum power point DC voltage
I_{actc}	Inverter total capacity in kWac
I_{acmp}	Inverter Maximum Power in Wac
n_i	Number of inverters

I_{dctc}	Inverter total capacity in kWdc
I_{dcmp}	Inverter Maximum Power in Wdc
$Euro_eff$	European weighted efficiency
CEC_eff	CEC weighted efficiency
P_{aco}	Maximum AC power output at nominal operating conditions
P_{dco}	Input DC power lever at which the AC power output is maximum
P_{so}	Power Consumption during operation
P_{nt}	Power Consumption at night
V_{ac}	Nominal AC voltage
V_{dcmax}	Maximum DC voltage
I_{dcmax}	Maximum DC current
$MPPT_{low}$	Minimum MPPT DC voltage
$MPPT_{high}$	Maximum MPPT DC voltage
V_{dco}	Nominal DC voltage
P_{ldc}	Total DC power loss
L_m	Loss by mismatch
L_{dc}	Loss by diodes and connections
L_{dcw}	Loss by DC wiring
L_{te}	Loss by tracking error
L_n	Loss by nameplate
L_{dco}	DC power optimizer loss
P_{dc}	Net DC array power
P_{lac}	Total AC power loss
L_{sut}	Step up transformer loss
P_{ac}	Net AC array power
V_b	Bank voltage
V_c	Cell nominal voltage
n_{cs}	Number of cells in series
c_c	Cell capacity
C_b	Bank capacity
c_c	Cell capacity
n_{cp}	Number of cells in parallel
c_c	Cell capacity
I_{maxc}	Maximum charge current
$C - rate_{cmax}$	Maximum C-rate of charge
I_{maxd}	Maximum discharge current
$C - rate_{dmax}$	Maximum C-rate of discharge
$WACC$	Weighted Average Cost of Capital

d_{real}	Real discount rate
d_f	Debt fraction
f_t	Federal Tax Rate
s_t	State Tax Rate
e	Effective rate
l	Loan rate
I_{rc}	Ground reflected irradiance
i	Incident angle
α	Solar altitude angle
a_s	Solar azimuth angle
β	Panel tilt angle
a_w	Panel azimuth angle
C	Sky diffuse factor
N	Analysis period in years
C_0	Project equity investment amount
ρ	ground reflected irradiance factor

Contents

1 Introduction

1.1 Objective

The objective of this work is project and evaluate the main characteristics parameters of solar energy collection systems to be installed on the San Jose State University Spartan Superway project prototype, which simulates an Automated Transit Network. It is located in San Jose, California, United States.

The Analysis should include monthly and annual energy production, considering local irradiance, system performance and electric load, as well as cash flow studies that consider system costs, taxes, federal and state investments, and electricity rates. The results of this work should be used by the Spartan Superway project in order to install a photovoltaic system that could supply electricity to run the prototype.

1.2 Motivation and limitations

Solar radiation at the Earth‘s upper atmosphere is 174000 terawatts. 30 percent of it is reflected back to space and the remaining power is absorbed by clouds, oceans and masses. The interaction between atmosphere and solar radiation refraction of the light, generation a spectrum that is mostly spread across the visible and near-infrared ranges, with a small part in the near-ultraviolet. (GOSWAMI *et al.*, 2000) The amount of solar radiant energy falling on a surface per unit area and per unit time is called irradiance. The mean extraterrestrial irradiance normal to the solar beam in the Earth‘s atmosphere is approximately 1.35 kW/m^2. Distance between Sun and Earth varies with time of the year because of the Earth‘s elliptical orbit, changing the irradiance by ± 3.4 percent during the year.

The radiant energy from the sun is distributed over a range of wavelengths, and the energy that reaches a unit surface per unit time within a particular spectral band is known as spectral irradiance. Figure 1.2 shows extraterrestrial spectral irradiance, which can be approximated by the spectrum of a black body at 5800 K(ORDONEZ S. YANG, 2014).

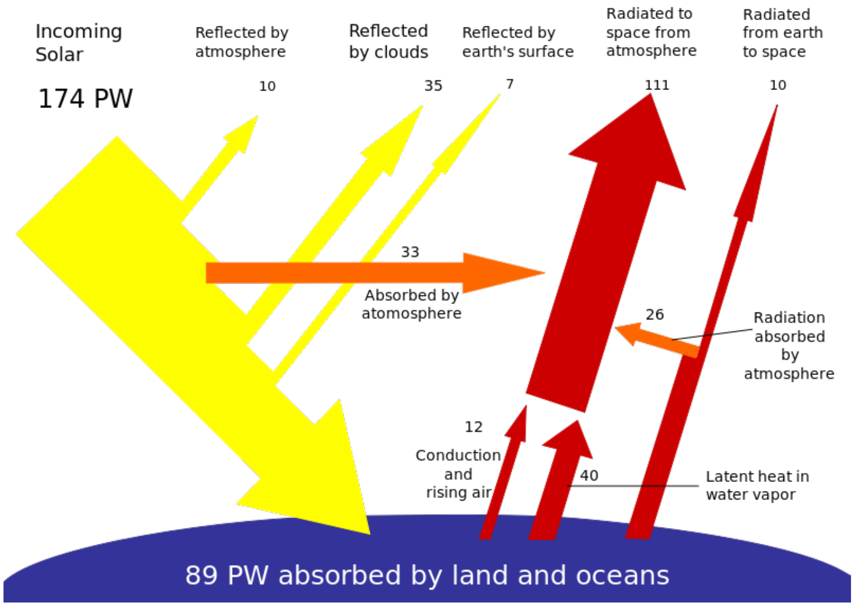

FIGURE 1.1: Solar radiation distribution.

There are three types of solar radiation at the surface: direct, diffuse and reflected. The first one, also called beam radiation represents the solar radiation that goes in a straight line from the sun down to the surface, having a definite direction. The diffuse radiation is the fraction of solar radiation that has been scattered by atmosphere molecules before getting to the surface, which means it does not have a definite direction. The proportion of diffuse radiation in the atmosphere increases with latitude and with less clear atmosphere conditions (caused by clouds or pollution, for example). For a clear sky and a sun high in the sky, the ratio between direct and diffuse radiation is about 85 percent to 15 percent. As the sun goes lower, this proportion keeps changing until it reaches about 60 percent to 40 percent when the sun is 10° above the horizon. At last, reflected radiation is the part of radiation that is reflected by the ground or the ocean(MASTERS, 2013). Beam radiation is measured by a peryheliometer, global radiation is measured by a pyranometer with a horizontal sensor and diffuse radiation is measured by a pyranometer under a tracking ball.

The majority of occupied places around the world receive between 150 and 300W per square meter of solar radiation, and the earth and its atmosphere receive continuously 1.7 x 10^{17} W of radiation from the Sun. A world population of 10 billion with a total power need of 10kW would require only 10^{11} kW. The amount of solar energy reaching Earth‘s surface in one year is about twice as much as will ever be obtained from all of the planet‘s non-renewable resources of coal, oil natural gas and mined uranium combined. Unfortunately, the nature of this energy has technical and economic limitations that are not clear from this macroscopy view of energy budget. Some problems are that the solar energy received is of small flux of density, intermittent and falls mostly in remote

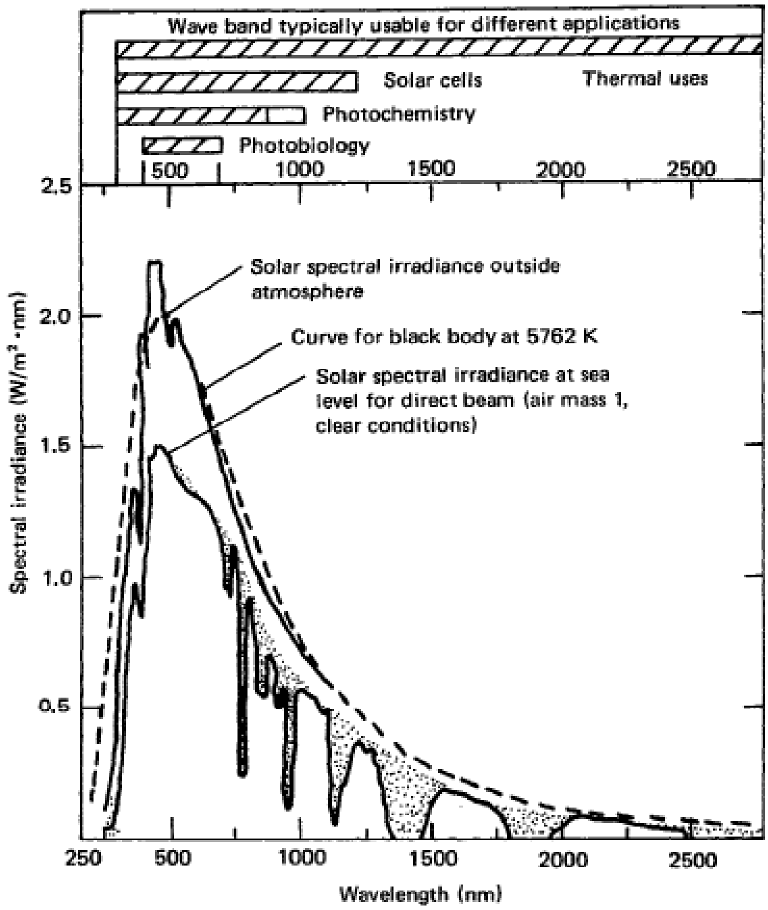

FIGURE 1.2: Spectral irradiance curves for direct sunlight extraterrestrially and at sea level with the sun directly overhead. Shaded areas indicate absorption due to atmosphere constituents, mainly H_2O, CO_2 and O_3. Wavelengths potentially utilized in different applications are indicated at the top.

places.(GOSWAMI *et al.*, 2000)

This potential is limited by latitude, weather, and time variation. Solar radiation is greater in regions closer to the equator (effect that can be minimized by using tracking systems for the case of photovoltaics panels). Clouds in the sky block the solar radiation and decrease solar panels performance. Time variation influences in the solar potential because there will be no energy to be absorbed by solar panels during the night. Another parameter to be considered for solar is the land availability. Solar panels can only be installed in unowned territory and it usually use big areas on the ground. One alternative way of setting up solar is using roofs as support for solar modules. Household owners that use solar technology can collect energy directly from their homes this way. It can also be used in parking lot roofs, which can be used both as shadow for the cars and power generator.(GOSWAMI *et al.*, 2000)

The low flux density makes necessary large surfaces to collect energy for large scale utilization, which makes costs for energy much higher. When the sun is overhead on a

FIGURE 1.3: Solar parking lot in Santa Cruz, United States.

cloudless day, 10 m^2 of surface could theoretically provide energy at a 10 percent efficiency of collection at the rate of 1 kW. Several losses reduce this amount of energy. 25 to 50 percent of this energy is lost by scattering and absorption in the atmosphere, even in cloudless places. Some is scattered back to space and some is absorbed by ozone, water vapor and carbon dioxide. Even on a clear day, diffuse radiation energy that can‘t be efficiently collected accounts for 20 percent of the total irradiance on a horizontal surface, and this percentage increases in places with clouds or pollution.(GOSWAMI *et al.*, 2000)

Ozone absorbs radiation at wavelengths below 300 nm and carbon dioxide absorbs radiation at wavelengths beyond 2500 nm, which limits Earth‘s irradiance to the range between 300 nm and 2500 nm. The second practical limitation is that most of the solar energy falls on remote areas that would demand transportation efforts to be useful to the industrialized nations. Table 1 maps global solar irradiance. The mean amount of energy available on a horizontal plane is greatest in continental desert areas around latitudes 25°N and 25°S of the equator. The highest annual mean irradiance is 300 W/m^2 in the Red Sea area. (GOSWAMI *et al.*, 2000)

Another limitation to the solar energy as a large-scale source of power and heat is its intermittency. Solar energy has a regular daily cycle due to the rotation of the earth around its axis and a regular annual cycle due to the inclination of the Earth axis with

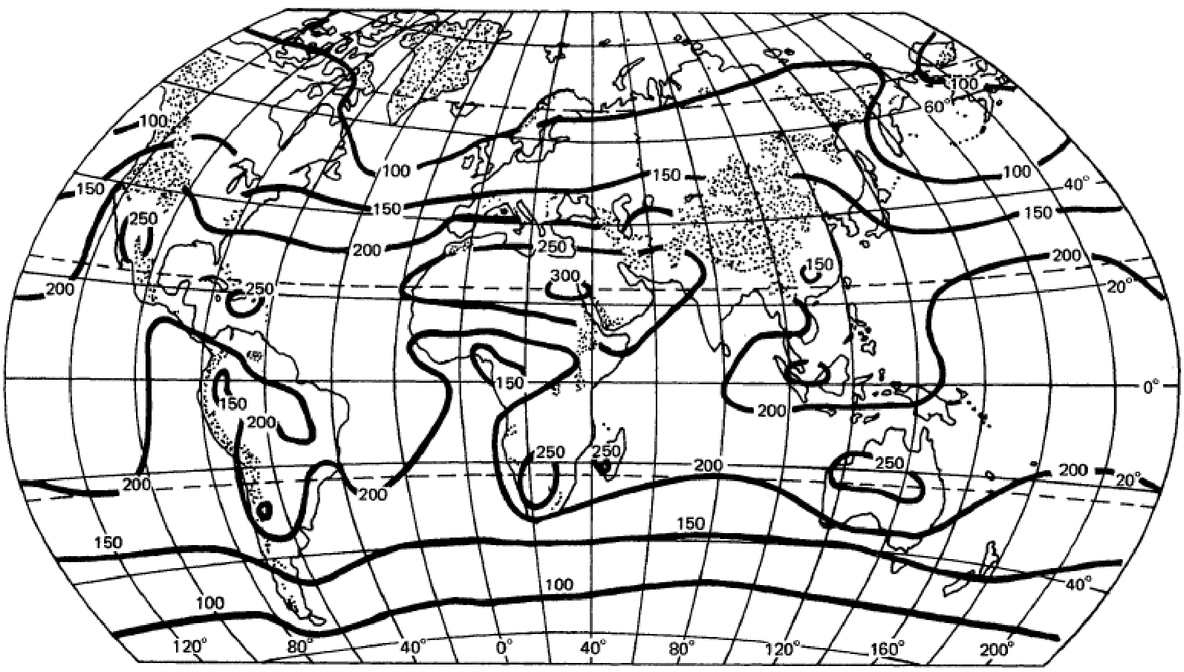

FIGURE 1.4: Annual global irradiance on a horizontal plane at the surface of the Earth (W/m^2 averaged of 24 hours)

the plane of the ecliptic orbit and because of the motion of the Earth around the sun. Bad weather is another factor that makes impossible efficient production of solar energy. Another variable to be considered in the use of solar energy is implementing satisfactory means of storing the energy once it has been collected. Figure 1.5 shows a list of storage means and its respective energy storage density.

Actually, there are some solutions for solar energy storage. For low-temperature storage, such as is necessary in heating and cooling buildings, sensible heat storage in water or rocks can be used. For electrical energy production systems, thermal storage at elevated temperature or electrochemical battery storage is currently being used. Another possible solutions that could be applied to solar energy storage are hydro storage, compressed-air systems in combination with gas turbines, thermal energy storage in liquid metal or molten salts, or using solar energy to generate hydrogen and storing it in gaseous or liquid phase, but the hydrogen production efficiency is relatively low and the cost of hydrogen storage and delivery systems is quit high nowadays.(GOSWAMI *et al.*, 2000)

Brazil has a great solar potential, having one of the biggest solar radiation ratings in the world. The majority of the Brazilian territory is located close to the equator, and there are no big variations in solar radiation along the year. The Northeast is the one that has the best potential for being the closest to the equator, with the biggest radiation area, which power is between 5700 and 6100 W/m^2 a day.(MAUTHNER WERNER WEISS, 2015) The worst irradiation in Brazil, in Santa Catarina, is 30 percent greater than Germany average

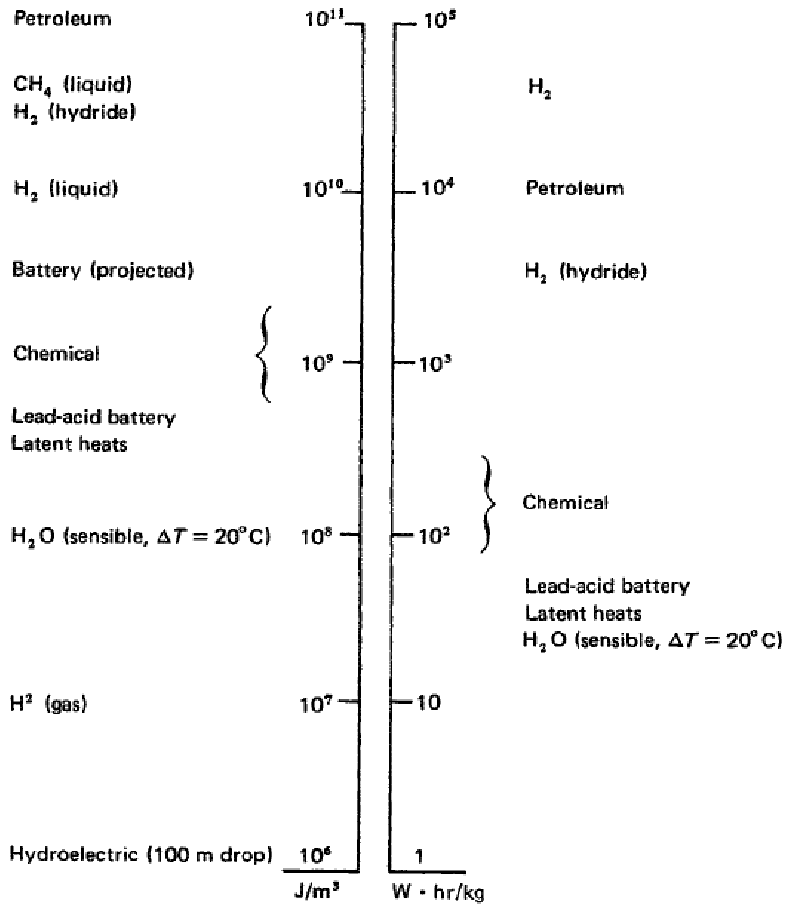

FIGURE 1.5: Mass and volumetric energy densities for typical energy storage media.

value, which shows this country's potential for solar development. In 2014, Brazilian solar thermal pharms produced 7.354 GWh in an area of 11240000 m^2 of collectors installed around the country. Photovoltaics market in Brazil is far from its potential. Power generated does not reach 35 MW. (SOLSTÍCIO..., 2013)

1.3 Historic and expected future

The first use of solar energy by humanity occurred in the 7th Century BC, when magnifying glasses were used to concentrate sun's rays to make fire and to burn ants. Greeks and romans used burning mirrors to light torches for religious purposes, and there is a story that Archimedes used the reflective properties of bronze to focus sunlight and set fire to wooden ships from the Roman Empire which were Syracuse. In 20 AC, Chinese documented the method of lighting torches using burning mirrors. Roman bathhouses of the 1st Century AC had large south facing windows to let the sun's warmth. In the 6th Century AC, sunrooms on houses and public buildings were very common.

In 1767, the scientist Horace de Saussure built the first solar collector, later used by Sir John Herschel to cook food during his South Africa expedition in 1830s. During Century XVIII, a lot of development was made for the solar energy technology.

In 1839, Edmond Becquerel discovers photovoltaic effect. Electricity generation in an electrolytic cell was increased when exposed to light. Some years later, in 1860s, August Mouchet developed the first solar powered steam engines. These engines became the predecessors of modern parabolic dish collectors. In 1873, Willoughby Smith discovered the photoconductivity of selenium and Charles Fritz described the first solar cell made from selenium wafers. Clarence Kemp patented the first commercial solar heater by the end of Century XVIII.

In the beginning of Century XIX, Albert Einstein published his paper on the photoelectric effect along with his theory of relativity, and it was proved in a Robert Milikan experiment in 1916. Later, in 1918, Jan Czochralski developed a way to grow single-crystal silicon. The photovoltaic technology is born in 1954 in the United States, when Daryl Chapin, Calvin Fuller and Gerald Pearson developed the silicon photovoltaic cell (PV). The first cell had 4 percent efficiency. Licenses to sell PV cells began to be sold in United States by Western Electric.

In the Mid-1950‘s, some laboratories of development of solar technologies were opened, like the world‘s first commercial office building using solar water heating and passive design, and research began to be made with the idea of developing photovoltaic cells for proposed orbit Earth satellites. In 1957, Hoffman Electronics achieved 8 percent efficient photovoltaic cells and 14 percent efficiency in 1960. N-on-P silicon photovoltaic cells appear in 1958.

In 1973, University of Delaware builds Solar One, one of the world‘s first photovoltaic powered residences. The system was a PV/thermal hybrid. The first amorphous silicon photovoltaic cells are fabricated in 1976 by David Carlson and Christopher Wronski. In 1977, the US Department of Energy launches the National Renewable Energy Laboratory (NREL), a federal facility dedicated to harnessing power from the sun. In 1980, the first thin-film solar cell exceeds 10 percent efficiency using copper/cadmium sulfide. The first solar powered car, the Quiet Achiever, is fabricated in 1982 in Australia. Also, 1982, US Department of Energy starts operating Solar One, a central-receiver demonstration project.

In 1986, the world‘s larger thermal facility, located in Kramer Junction, California, was commissioned. It contained rows of mirrors that concentrated the sun‘s energy onto a system of pipes circulating a heat transfer fluid. University of South Florida develops 15.9 percent efficient thin-film photovoltaic cell made of cadmium telluride. In 1994, NREL builds the most energy-efficient of all US government buildings worldwide and develops a solar cell (made from gallium indium phosphide and gallium arsenide) that becomes the first one to achieve 30 percent efficiency. In 1996, US department of energy begins operating an upgrade do Solar One, called Solar Two. In 1999, NREL achieves 18.8 percent efficiency for thin-film photovoltaic cells.

The researches in solar cells are being stimulated by the problem of the conversion efficiency and the cost of material. Nowadays, it is studied the solar photovoltaic technology using different materials such as polycrystalline silicon and amorphous, gallium arsenide, cadmium sulfide and others. The knowledge about the silicon technology, mainly the monocrystalline, and the abundance of this material make it predominant in the process of technology development.

The expectations to the future are to lower the price of photovoltaics to be competitive with traditional sources of electricity within 10 years, and to use solar electricity to electrolyze water, producing hydrogen for fuel cells for transportation and buildings. All buildings will be built to combine energy efficient practices for a net-zero energy building, producing its own power supply(U.S DEPARTMENT OF ENERGY, 2002).

1.4 Types

There are two main types of solar collection technologies: photovoltaic, which converts energy from the sun directly into electricity, and solar thermal, which uses solar energy to heat an appropriate fluid. There are also hybrid systems that use both types of technology to collect energy from the sun. The next sections will explain these two of energy collection, with more details to photovoltaics, which is the focus of the work developed in this document.

1.4.1 Photovoltaics

The energy conversion principle used by this type of technology is the photovoltaic effect, discovered by Edmond Becquerel in 1839. There are materials called semiconductors, which have a valence band totally filed with electron and a conduction band totally empty in low temperatures. Figure 1.6 shows a photovoltaic cell mechanism: In a semiconductor, the separation between two bands, or the energy gap, is approximately 1 eV, which make then different from nonconductors that have much greater energy gaps. Semiconductors have special properties. One of them is the increase of conductivity with temperature, because of the thermal excitation of electrons from the valence band to the conduction band. Photons in the visible band that hit a photovoltaic cell with energy superior to the material gap, bring electrons to the conduction band, but to make the photovoltaic effect

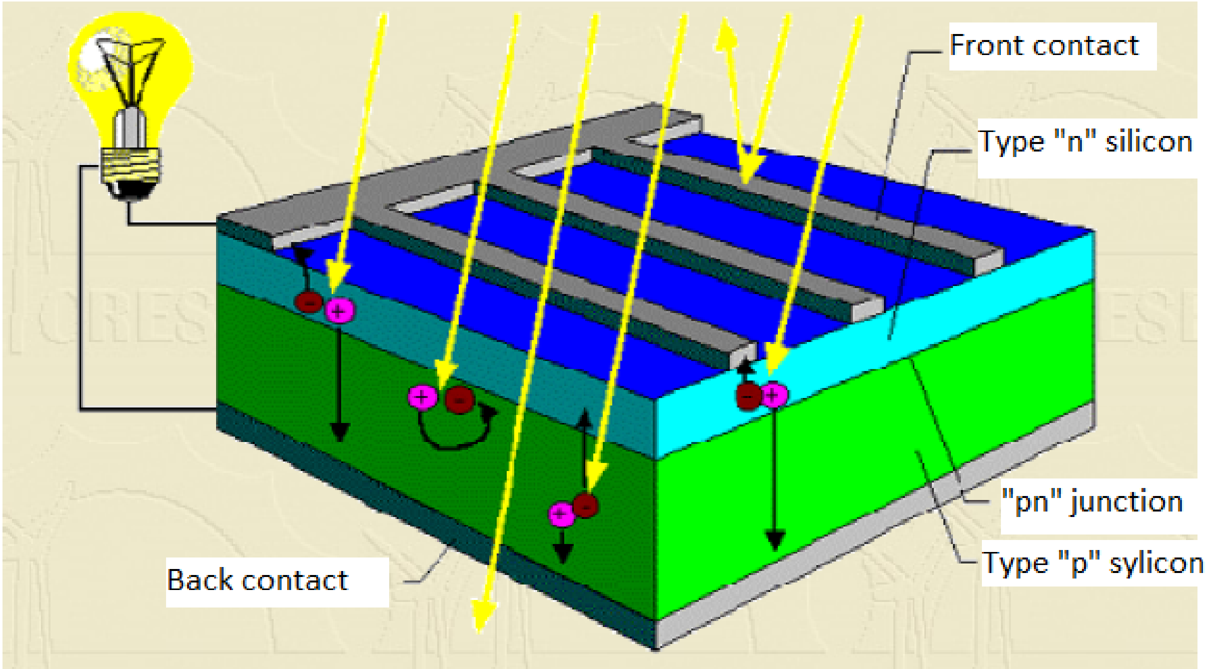

FIGURE 1.6: Photovoltaic Cell composition.

happen, it necessary and appropriate structure for the electron to be collected, generating current.

The most used material in photovoltaic cells is silicon, which atoms have four electrons in the valence band that make bonds with the nearest electrons, making a crystalline structure. Phosphorus has five electrons in its valence band, so if it is added to a silicon structure, it will have one extra electron that cant be paired. With thermal energy, this electron can be easily moved to the conduction band. That is why phosphorus can be considered a n dopant. In the other side, boron has three electrons in its valence band, so if it is added to the silicon structure, there will be a lack of one electron to complete the four bonds of silicon and a gap will be created. This gap can move free in the structure, conducting this lack of electron among the silicon structure. That?s why boron can be considered an p dopant.

The photovoltaic cell is composed of two pieces of silicon put together. One of them is with an n dopant and the other one with p dopant, what is called pn junction, like shown in figure 5. In this configuration, electrons move from the n side to the p side and gaps move in the opposite way, generating an accumulation of electrons in the p side and gaps in the n side. This accumulation creates an electric field that is opposite to the movement of electrons and gaps in the pn junction. When the electric field is strong enough to stop the movement of electrons and gaps, an electrostatic equilibrium is established. This situation is shown below in figure 1.7. Photons with more energy than the gap between valence band and conduction band will create a pair electron-gap,

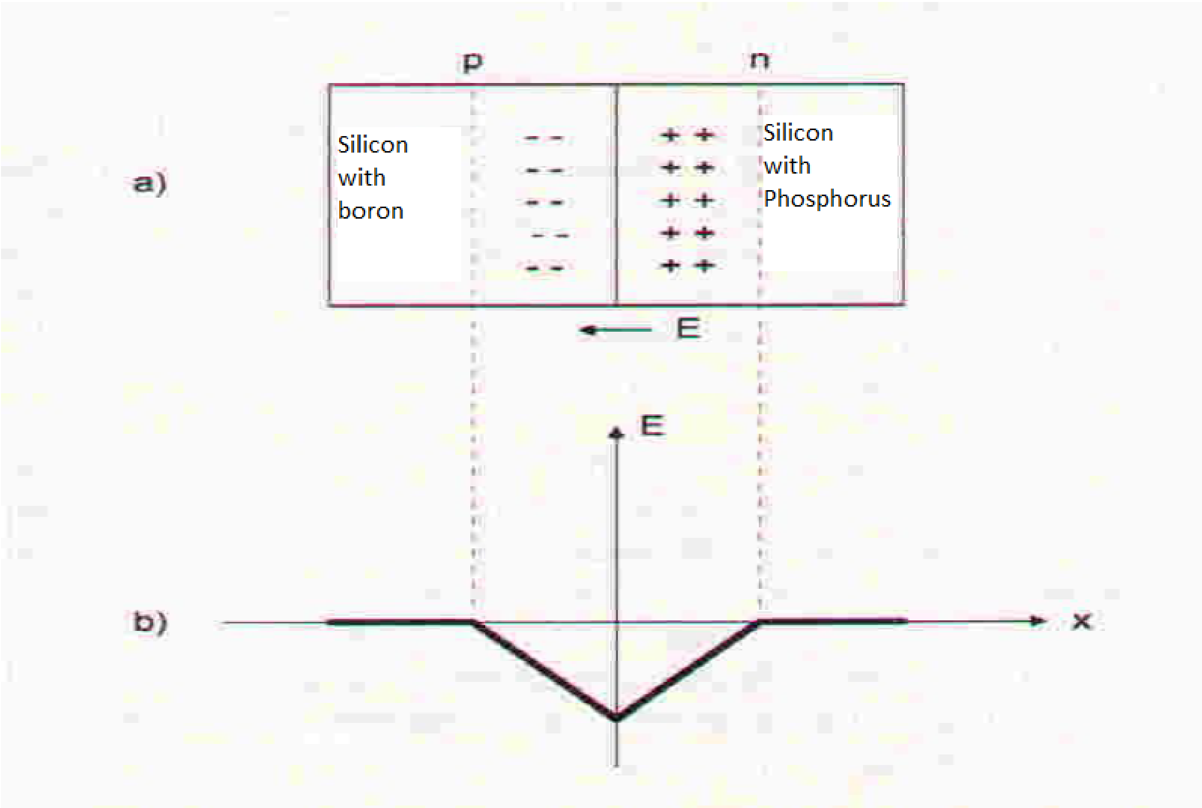

FIGURE 1.7: (a) PN junction with accumulation of electrons in p side and gaps in n side. (b) Electric field generated by motion of electrons and gaps.

which will accelerate electric charges if it happens in a region where the electric field is not zero, generating electric current. This phenomenon is called photovoltaic effect. In a photovoltaic device (figure 1.8), free electrons generated by receiving photons can pass through an external resistance, recombine with positive holes in the n-side or move toward the p side, which is prevented by the opposite electric field. Usually, the n layer is extremely thin, decreasing the mobility of electron in the lateral direction and, therefore, the probability recombination inside the n-side(FADIGAS, 2000). Energy contained in a photon is given by:

$$E_p = h\nu. \tag{1.1}$$

Where h is the Plank‘s constant, 6.625 x $10^{(} - 34)$ J/sec and ν is the wave frequency, which can be related to the wave length λ and the speed of light c as:

$$\nu = c/\lambda \tag{1.2}$$

Therefore:

$$E_p = hc/\lambda \tag{1.3}$$

For silicon, which has a gap of 1.11 eV, the wavelength necessary to bring electrons to the

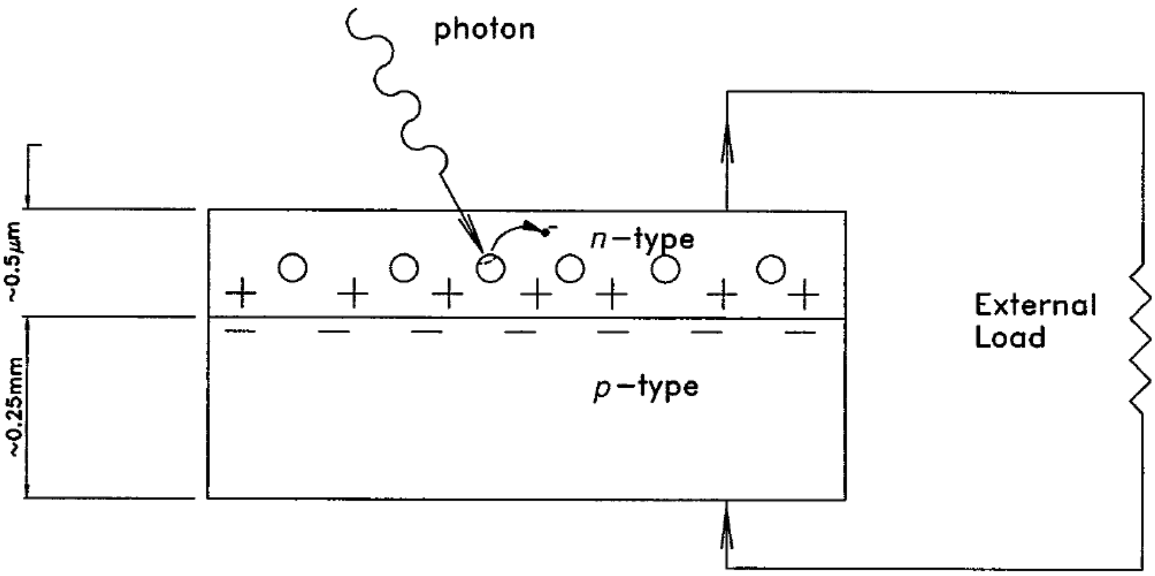

FIGURE 1.8: Schematics of a photovoltaic device.

conduction band is 1.12 μm.

A photovoltaic cell can be electrically modelled by the following seven-parameter circuit in figure 1.9(FADIGAS, 2000)(BIKANERIA SURYA PRAKASH JOSHI, 2013). The parameters in the circuit shown are defined as:

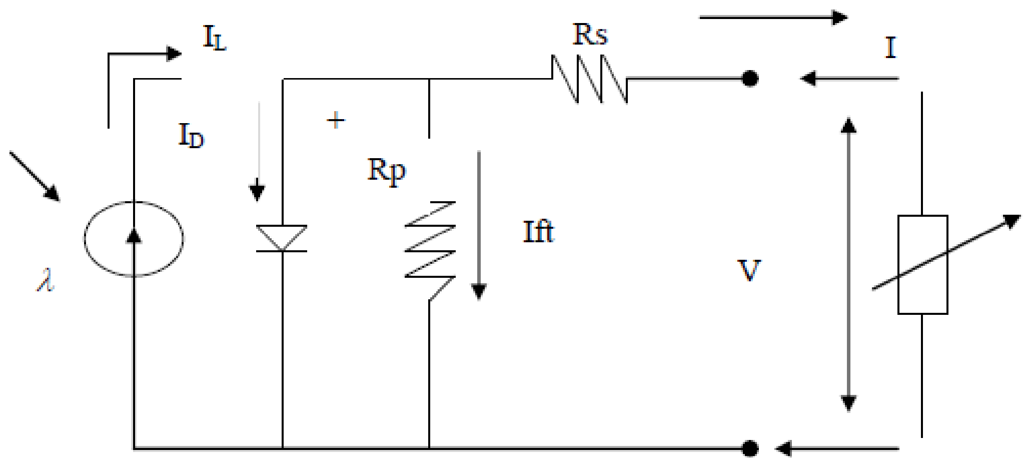

FIGURE 1.9: Equivalent electrical circuit for a photovoltaic cell

- I_L - Current generated by radiation;
- I_D - Saturation current of the diode;
- I - Current generated in the terminals;

- I_{ft} - Leakage current to ground;
- R_P - Parallel Resistance;
- R_S - Series Resistance;
- A - Curve correction parameter;

In fixed temperature and radiation, I is given by:

$$I = I_L - I_D(e^{[\frac{V + IR_S}{A}]} - 1) - \frac{V + IR_S}{R_P} \tag{1.4}$$

R_S represents internal resistance and it depends on thickness, impurity in the material and resistance of the contact, and R_P is the resistance to current going to the ground. In an ideal case, R_s=0 and R_P is infinite(BIKANERIA SURYA PRAKASH JOSHI, 2013).

Two important parameters in the electrical analysis of a photovoltaic cell is the open circuit voltage (V_{oc}), which is the potential difference between the terminals when the cell or a group of cells (module) are exposed to the sun with no load connected to it, and the short circuit current (I_{sc}), which is measured putting the terminals in short circuit with the cell (or module) exposed to radiation. I_{sc} is approximately equal to I_L because the values of I_D and I_{ft} are too low. V_{oc} can be expressed by the following equation:

$$V_{oc} = V + IR_p \tag{1.5}$$

A cell is characterized by its current versus tension, which is exemplified in figure 1.10. The par current-voltage changes with the load applied to the photovoltaic cell. For this cell, the current is approximately constant until 0.5 volts. After that, diode current starts to get higher values. In open circuit, all the current generated is passing through the diode and the parallel resistance, and the voltage is 0.6 V. In a silicon cell of 1 cm^2, in a solar radiation of 1000 W/m^2, there is an open circuit voltage of 0.6 V and a short circuit voltage of approximately 20 to 30 mA. The power generated by a photovoltaic cell is shown in figure 1.11. It‘s numerically equal to the product of current and voltage. The curve of current is shown in the same plot. As power generated by a single cell, industries usually manufacture modules of cells in parallel and series to generate greater power by module. The efficiency of a cell or module is the result of the quotient between the power output of it and the power contained in the solar radiation received by it. Changes in irradiance influence current curve and efficiency. The variation in efficiency and current produced decreases as irradiance increases. This behavior is shown in figures 1.12 and 1.13. Temperature increases produces linear increases in I_{sc} and linear decreases in V_{oc}. If I_{sc0} and V_{oc0} are the are the short circuit current and the open circuit voltage in a reference temperature T, α and β are respectively the temperature coefficients and of I_{sc}

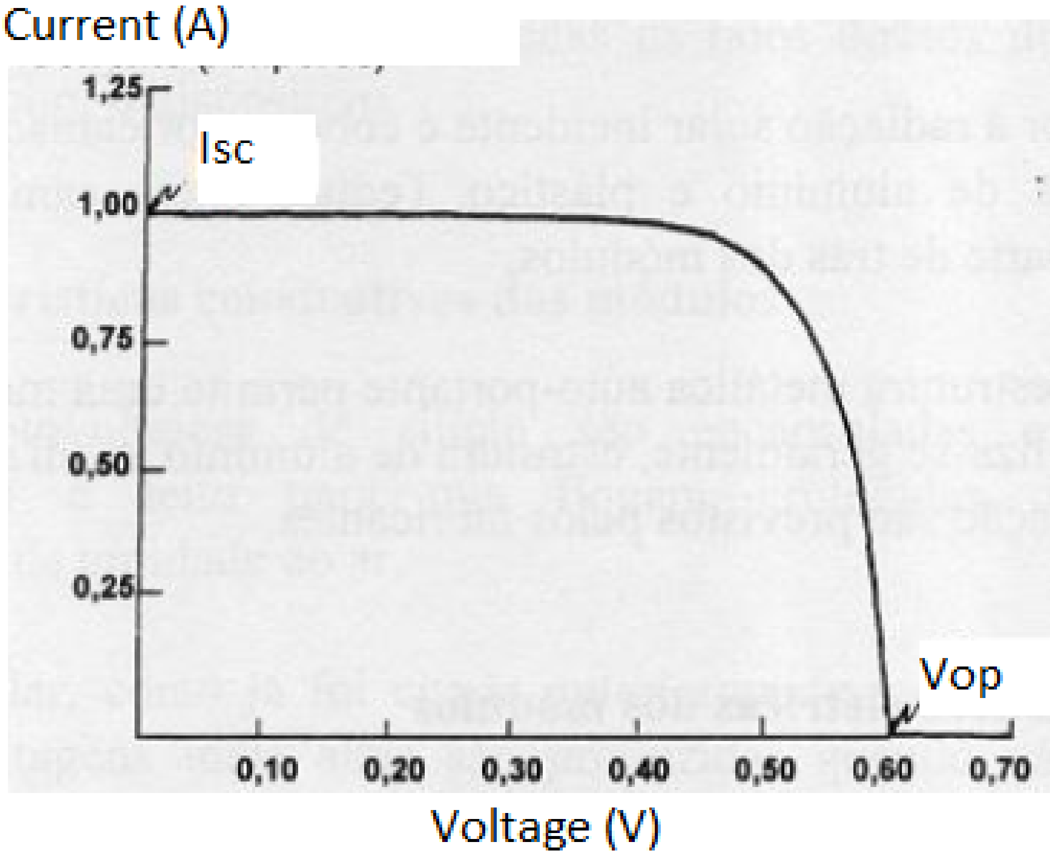

FIGURE 1.10: Curve I x V of a typical cell

and V_{oc} and the temperature varies in ΔT, the following equations can be applied:

$$I_{sc} = I_{sc0}(1 + \alpha\Delta T) \tag{1.6}$$

$$V_{oc} = V_{oc0}(1 + \beta\Delta T) \tag{1.7}$$

Therefore, the power output can be expressed by the following equation:

$$P = VI = I_{sc0}(1 + \alpha\Delta T)V_{oc0}(1 + \beta\Delta T) = P_0(1 + \alpha\Delta T)(1 + \beta\Delta T) \tag{1.8}$$

These equations can be graphically verified in plots shown in figures 1.14 and 1.15. For each temperature, there‘s a different power curve with a peak value that occurs in a different voltage. The project of the photovoltaic system needs to catch the maximum power in all the range of temperatures, changing the output voltage in order to achieve it. This function is made by the maximum power point tracker, an electronic component that is included in the design of the photovoltaic system that catches the voltage and the output

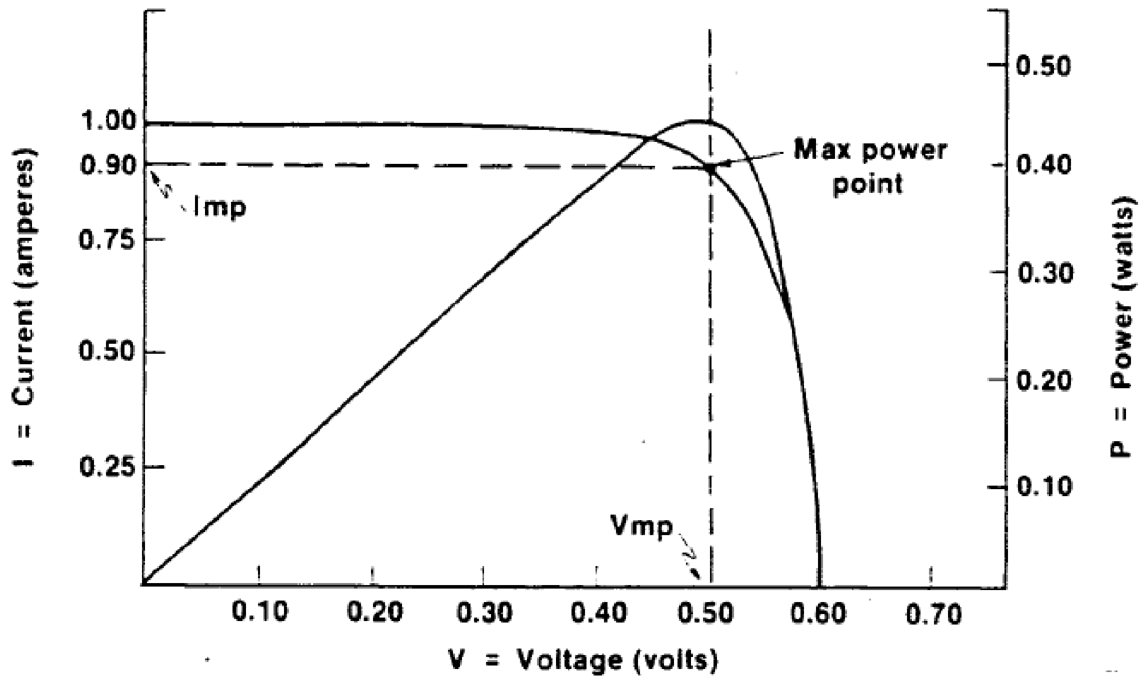

FIGURE 1.11: Typical current, voltage and power characteristics of a solar cell

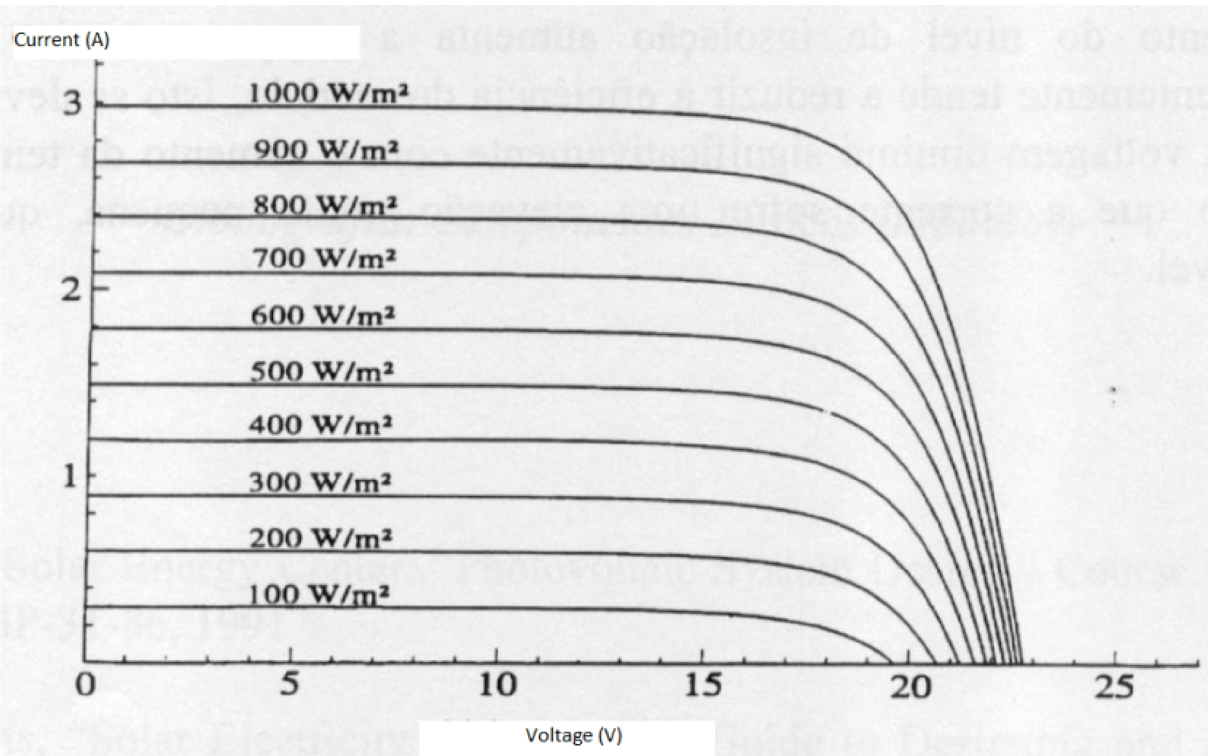

FIGURE 1.12: Curve V x I for various solar irradiances

current and continuously changes the point of operation to achieve maximum power under different climatic conditions. Figure 1.16 shows a basic photovoltaic system, which can be

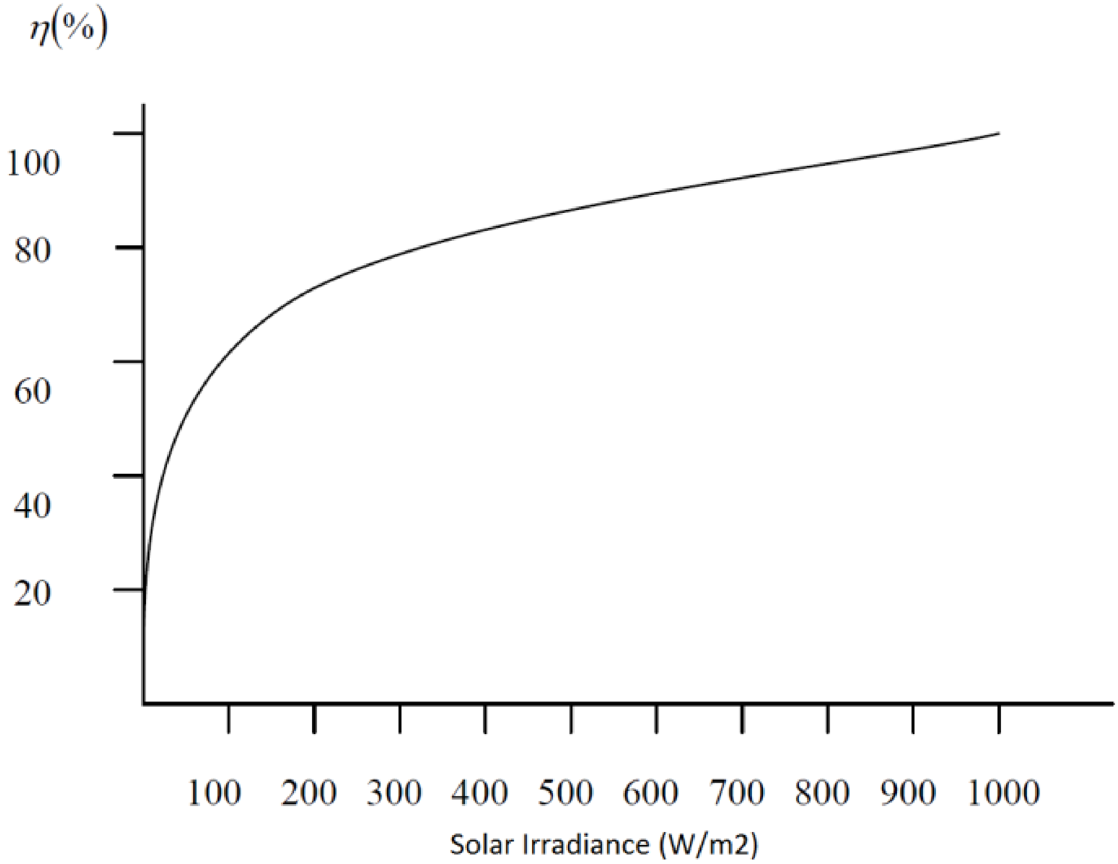

FIGURE 1.13: Efficiency variation with irradiance

used to charge a battery or to give power to an appropriate load. The system also includes an inverter, a dispositive that converts DC current that comes from the module into AC current to be used in a load(FADIGAS, 2000). There are three main different types of solar panels out on the market: monocrystalline silicon solar panels, polycrystalline silicon solar panels, and thin-film solar cells, each one with specific characteristics that are important to consider when choosing a solar cell. Some important attributes to analyze cost, efficiency, life span, simplicity for manufacturing and space occupied by solar panels (TEAM, 2015).

Monocrystalline silicon solar panels are made of high-purity silicon, with very well aligned molecules. This alignment helps the solar cell to convert solar energy into electricity better, giving monocrystalline solar panels the highest efficiency rate of about 15 to 20 percent. These types of solar cells are the most space efficient ones, have long life spans and have a good performance in low conditions, but are the most expensive of the three types, because of the price of high-purity silicon. Figure 1.17 shows a monocrystalline silicon solar panel. Polycrystalline silicon solar panels use raw silicon that is melted and poured into a square mold, being simpler to make and cheaper than monocrystalline panels. In the other hand, the efficiency is typically 13-16 percent, which is less than the

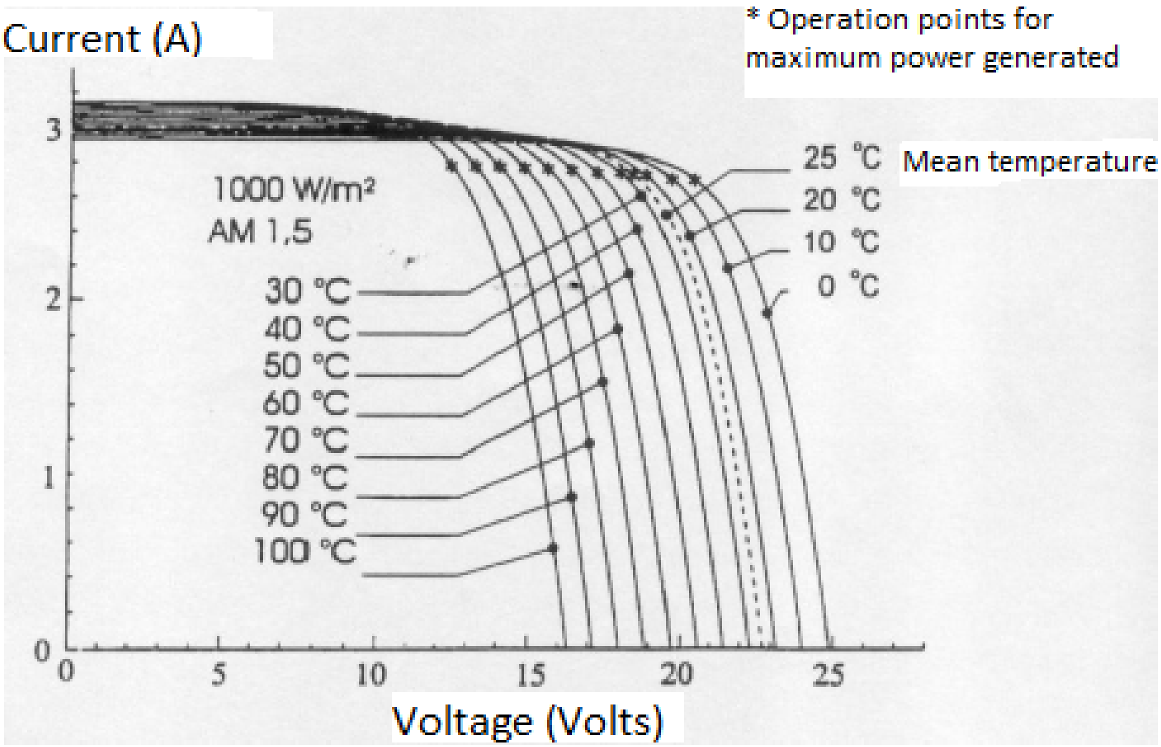

FIGURE 1.14: Curve V x I for various temperatures.

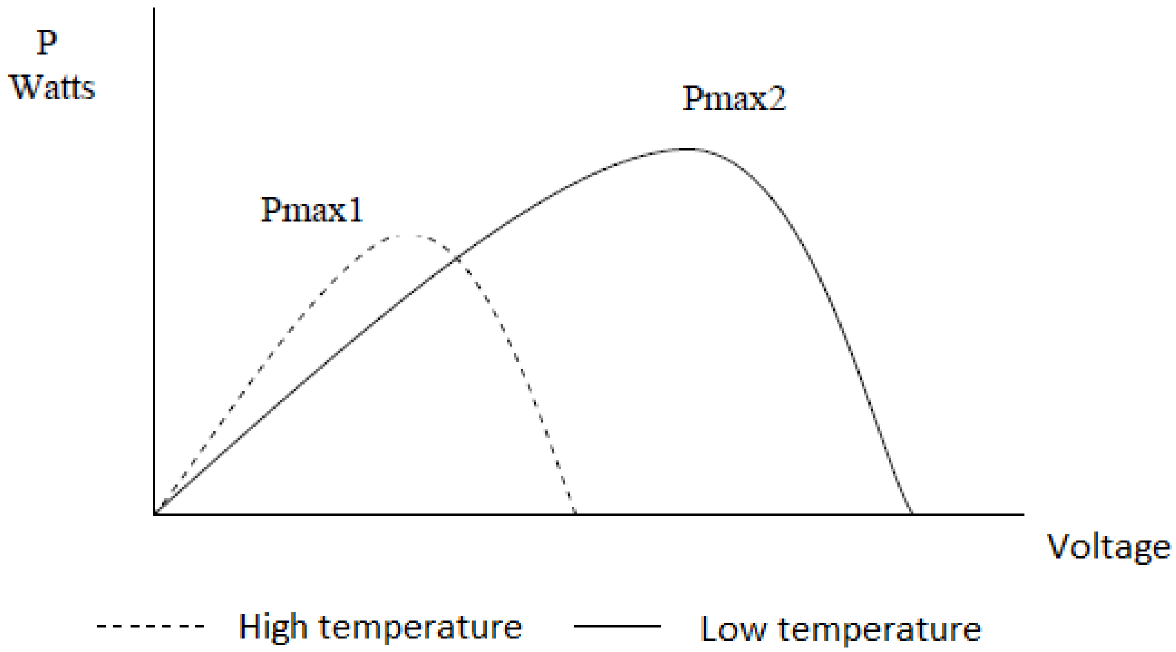

FIGURE 1.15: Power curve for different temperatures.

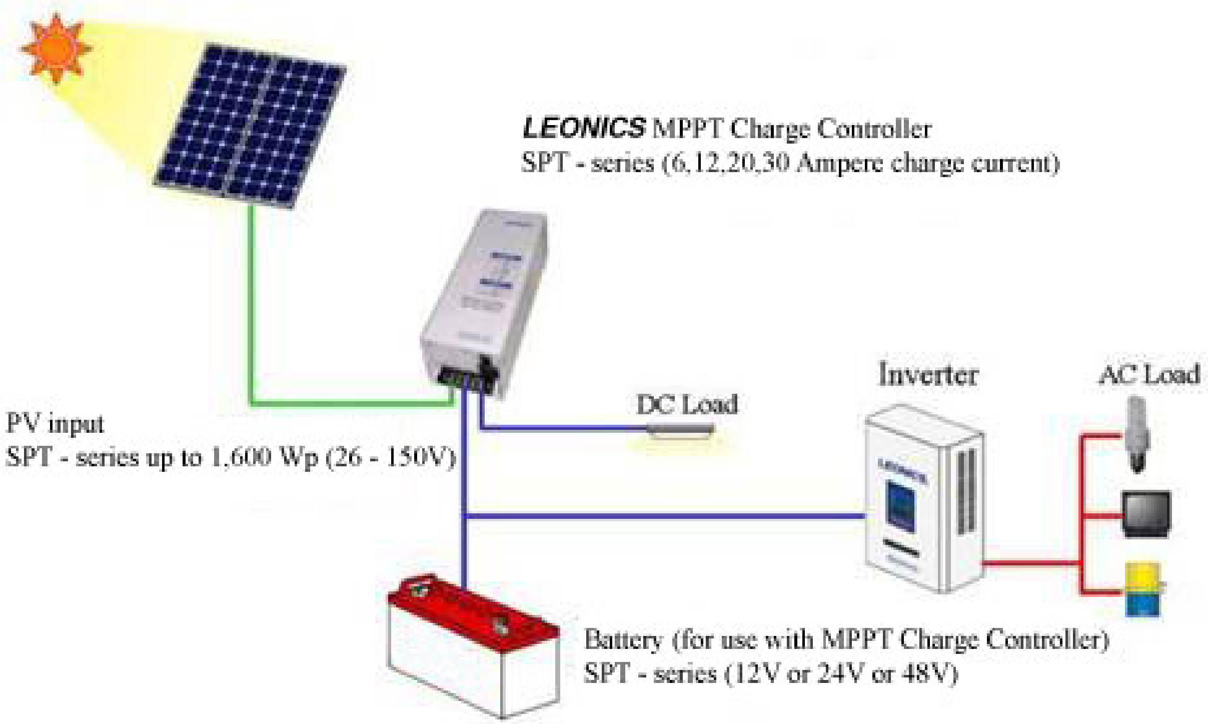

FIGURE 1.16: Example of basic photovoltaic system sketch.

FIGURE 1.17: Monocrystalline Silicon Solar Panel.

monocrystalline panel, so more space would be filled with solar panels to generate the same power output as monocrystalline panels would generate. The polycrystalline silicon solar panel is shown in Figure 1.18. Thin-film solar cells are made from depositing one or several layers of photovoltaic material onto a substrate. This is the cheapest option as the panels are mass-produced. These types of panels are able to bend as well. The efficiency rate is only 7-13 percent. They also tend to degrade faster than monocrystalline

FIGURE 1.18: Polycrystalline Silicon Solar Panel.

and polycrystalline solar panels. The thin-film solar cell is shown in Figure 1.19.

FIGURE 1.19: Thin-film Solar Cell.

1.4.2 Solar Thermal

Solar Thermal collectors use incident solar radiation to produce heat in a useful temperature. This technology has several applications nowadays, like heating swimming pools, cooking, or creating steam for electricity generation.

The basic mechanism consists in exposing the collector to solar radiation to heat the fluid inside it. The performance is obtained by measuring inlet and outlet temperature and fluid flow rate. The useful heat gain,q_u, can be computed with the following equation:

$$q_u = \dot{m}C_p(T_{f,out} - T_{f,in}) \tag{1.9}$$

Where $\dot{m}$ is the mass flow rate of the fluid, C_p is the specific heat and $T_(f, out)$ and $T_(f, in)$ are the outlet and inlet temperature, respectively. The instantaneous efficiency of the collector, η_c, can then be expressed as:

$$\eta_c = \frac{q_u}{I} \tag{1.10}$$

Where q_u is the useful heat gain and I is the total radiation received by the collector. For a flat plate collector, the total radiation is given by:

$$I = I_c A_c \tag{1.11}$$

Where I_c is the local irradiance and A_c is the collector area. Figure 1.20 shows a flat plate solar thermal collector. There are many types of collectors, which can use reflection or refraction of light to concentrate solar radiation and increase solar performance, for example, the parabolic trough concentrator, consisted of a parabolic shaped mirror that concentrates rays into its focus, where the heat transfer fluid flows, like shown in figure 1.21.

1.4.3 Automated Transit Network

An Automated Transit Network (ATN) is a transportation system composed by vehicles and guideways that contains the following specific characteristics (Carnegie, Voorhees, and Hoffman, 2007): vehicles controlled automatically that travel to their destination without human control, on-demand service (the vehicles only arrives when summoned, instead of having a predetermined schedule), supervisory safety and availability monitoring (the vehicles and subsystems are continuously monitored), non-stop service to the destination (because it uses off lines stations, which means that the stations are not on the main line of transit) and a discrete guideway, separate from the streets. A Personal Rapid Transit (PRT) is a subset of ATN focused on smaller vehicles, which are more similar to

FIGURE 1.20: Solar thermal flat plate collector.

FIGURE 1.21: Parabolic Trough Concentrator. The tube is in the focus of the parabola and contains heat transfer fluid.

the automobile. These ones have the following additional characteristics: small vehicles with one to six riders, vehicles able to function around tight turns, light weight vehicles, which minimizes requirements for energy supply and guideway support, and private ridership. It uses a guideway network in which the vehicle can move around, getting to the destination non-stop and without a predetermined schedule(TEAM, 2013). In the current days, there are five ATN operating around the World, which are the Morgantown PRT, in West Virginia, USA , the ParkShuttle, in the Netherlands , the Cyber Cab, in Masdar City, Abu Dhabi, United Arab Emirate , the ULTra PRT, in London Heathrow Airport, United Kingdon, and the Vectus, in Suncheon Bay, South Korea.

FIGURE 1.22: Example of ATN with its vehicles moving above the guideway.

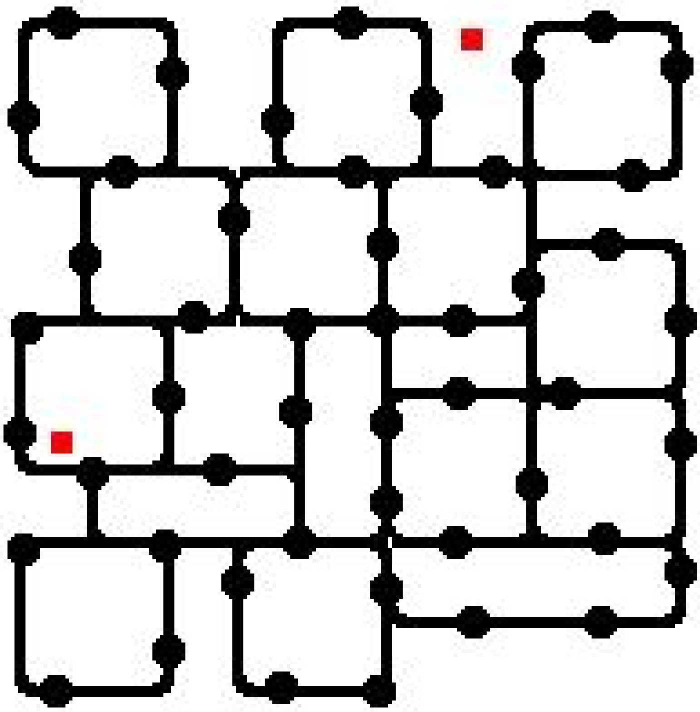

FIGURE 1.23: Example of network used by an ATN for transportation. The red points represent the initial and final positions of the riders. The black points represent the stations.

1.4.4 Spartan Superway Project Overview

The Spartan Superway is a solar powered Automated Transit Network designed to provide an alternative to both personal automobile and public transportation. Actual mass transportation systems have higher maintenance and construction costs than ATN systems, with bigger waiting and travel times because of the stops along the way. The

Spartan Superway consists in a sustainable solution to traffic problems in urban and suburban areas. The design was divided in six engineering components: cabin, propulsion, structure and guideway, solar energy, control systems. The designed cabin should fit four adults and have approximate interior of 80 in of length x 52 in width x 69 in height. The cabin goes suspended from the guideway in a minimum height of 14 feet. The structure of the guideway is supported by columns made of A574 grade 50 steel an spaced 10-50 ft apart and the guideway is to be a Prat truss(TEAM, 2013). The solar panels to be used are of the Miasole Thin Film type. The choosing of this type of module was motivated by the fact that Miasole (a solar panel manufacturer company) had a partnership with the project, and it would give any necessary thin film solar panels to the photovoltaic system building. Control, schedule and routing of the vehicles use a centralized system that coordinates semi-autonomous systems.

2 Project Development

2.1 Internship Overview

The Spartan Superway is a San Jose State University project that started in 2013 which consists of a suspended ATN that moves under a guideway powered by solar panels. The project team is composed by students divided by teams, which are: bogie team, solar team, controls team, cabin team and guideway team. During the summer of 2015, the author of this document worked in the solar team with the goal of improving the solar configuration for this system. The idea was to use the guideway as a base to the solar configuration to be designed and installed. In the beginning, studies were made to learn what have already been done in the project during the years of 2013, 2014 and 2015, and what could be improved in the solar design.

The students working in the project have built two models of the transportation system: a full scale model (figure 2.1) and a smaller prototype, called small scale model. The particular goal of the author was to design different configurations for the solar in the full scale model, simulate them in NREL (National Renewable Energy Laboratory) - SAM (System Advisor Model) and then choose the one with the best performance, economic and esthetic characteristics. The chosen design would be built above the full scale model and then connected to the vehicle using the appropriate circuit equipment, with inverters, charge controllers and batteries. In the beginning, the full scale model had two solar panels on the top, one of them attached to a frame with an actuator that could make the structure rotate following an ARDUINO program routine, and the other one fixed, like shown in figures 2.2 and 2.3. The following sessions will show the drawings of the designs, that were made in Dassault Systems Solidworks, the simulations made on NREL-SAM and the conclusions that could be extracted from this analysis.

2.2 Drawings

The author could get the Full Scale drawings from other students of the project and work on the solar configuration for it. One of the project sponsors is the Thin Film Module

FIGURE 2.1: Full Scale Model.

Manufacturer Miasole, which had 4 available types of solar module that are shown in figure 2.5:

- FLEX-02N - Dimensions: 102.3 in x 14.6 in;
- FLEX-02NS - Dimensions: 67.8 in x 14.6 in;
- FLEX-02W - Dimensions: 102.3 in x 39.4 in;
- FLEX-02WS - Dimensions: 67.8 in x 39.4 in;

All of these modules were flexible, so it was necessary to design a frame to be used as a backing for the panels. The team agreed that it would be better to keep the modules plane and tilted in a specific angle, to minimize cosine losses and to avoid water and dust accumulation on the panel. The model designed would use fixed panels to simplify the following manufacturing working and to minimize costs. For fixed panels there is an expression that optimizes the power output(OPTIMUM..., 2015):

- For latitude below 25°, use the latitude times 0.87.

FIGURE 2.2: Stion rigid solar panel that can be rotated by an actuator.

- For latitude between 25° and 50°, use the latitude, times 0.76, plus 3.1 degrees.
- For latitude above 50°, there are other factors to consider.

The latitude of San Jose is 37.33°, so the optimal tilt angle would be 31.22°. The drawings made used the types of modules mentioned above, using its dimensions to see the best geometric disposition for each panel. The designs made were the following. The goal of the solar design was to cover the trail as much as possible in such a way that optimizes power, energy and cost.

Design 1 consists of 16 solar panels of the FLEX-02N type being supported by a metal frame with a tilt angle of 31.22°. It does a good job on covering the trail on the left part of the trail, but it shows the guideway on the right. It would not be convenient to put panels on the right side because they would be shaded by the other left ones.

Design 2 does have a disadvantage and an advantage compared to the others. The disadvantage is that it has vertical and horizontal panels, with a tilt angle that is not optimal, and the advantage is that all panels are oriented in the same direction, so the simulation can assume that they are all facing South, which is better for the system performance. One of the panels on the top is almost horizontal, so it won‘t shade the panels behind it. They are not totally horizontal to avoid accumulation of water from the

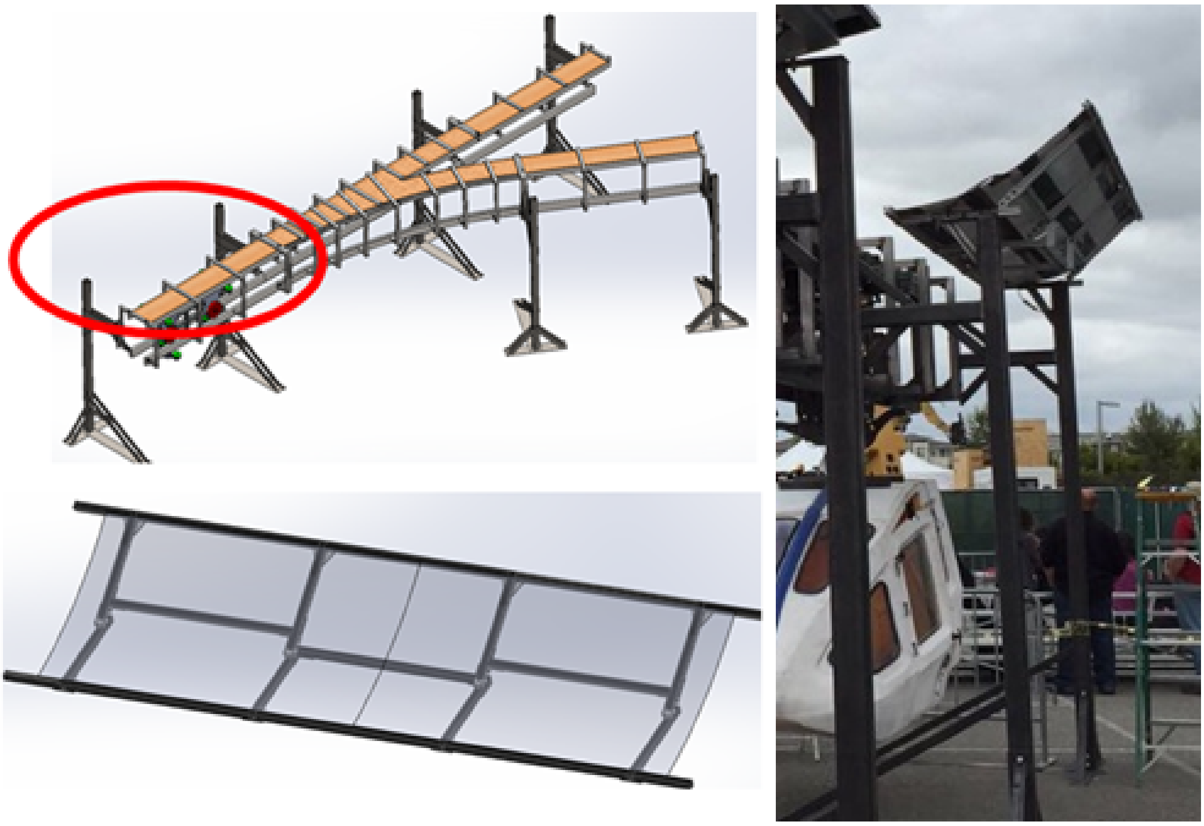

FIGURE 2.3: Miasole Thin Film Module fixed by a metal frame.

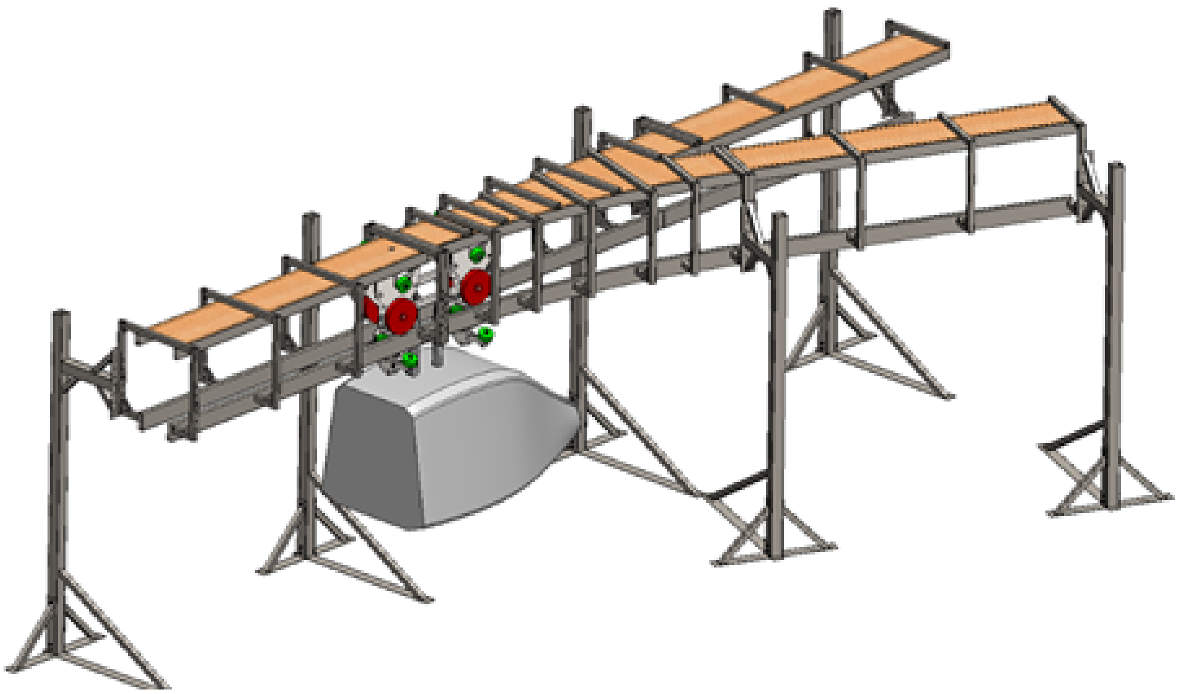

FIGURE 2.4: Full Scale Model Drawing in SolidWorks.

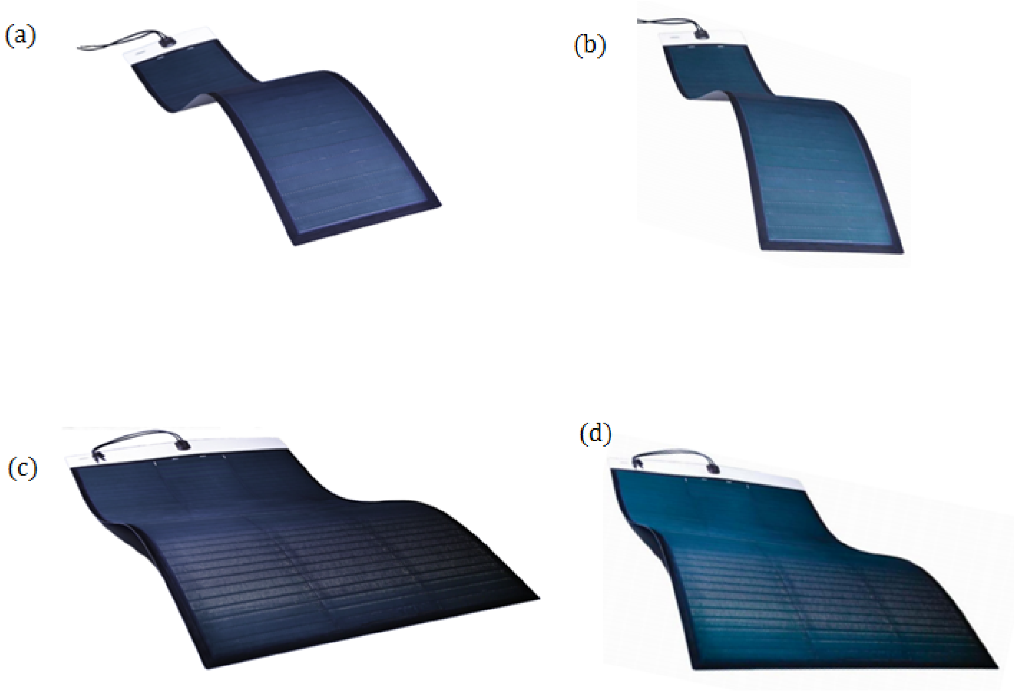

FIGURE 2.5: Available Solar Modules.(a) is the FLEX-02N Module, (b) the FLEX-02NS Module, (c) the FLEX-02W module and (d) is the FLEX-02WS module

rain on the top of it.

Design 3 uses all the types of the available solar panels. The blue ones are of the FLEX-02NS type, the green ones of the FLEX-02N type, the brown ones of the FLEX-02W type, and the gold ones of the FLEX-02WS. This design is very good for covering the sides of the trail even though there is a higher setup costs because more supports have to be built. The gray plate is a metal sheet that goes behind the panels to be used as a backing. The panels would be attached to the sheet by using clamps.

Design 4 is a more complex design with supports on the side of the rail. The panels are of the FLEX-02N type. It is similar to the first one in terms of power output, because it has the same number of modules disposed in the same geometric position, but it would be more difficult to install this one, because more supports would be needed.

2.3 Initial Considerations

SAM does not support systems with different types of modules, so it was not possible to simulate the third solar design. The solar array 4 has the same performance characteristics as the solar array 1, because it has the same kinds of subarrays: one of then with 12 modules FLEX 02N at azimuth 180° with tilt angle 31.22° and other one with 4 modules FLEX 02N at azimuth 23.62° with tilt angle 31.22°. As the calculations are not considering shading losses, the results for the analysis would be the same for both designs.

2.4 Simulations

2.4.1 Location and Resource

The simulations were made using the software NREL - SAM and they evaluated performance and cost characteristics of the solar configurations made. The initial interface of the program is the one shown in figure 2.9.

The parameters shown in the left side of figure 2.9 can be configured for any solar configuration to be simulated. In our case, the parameters that change between solar configurations are the System Design and the Module. The remaining system characteristics were configured as the following:

- Financial Model: Commercial System

In SAM, Residential and Commercial Systems buy and sell electricity at retail rates and displace purchases of power from the grid. PPA (Power Purchase Agreement) projects sell electricity at a wholesale rate to meet internal rate of return requirements.

- Location: USA CA San Jose International Airport

SAM uses a weather file from its database for the chosen location to calculate irradiance through the months. Figure 2.11 shows hourly global, beam and diffuse irradiance in W/m^2 in San Jose International Airport used for SAM calculations. The Source of the weather files is NREL-TMY3 (Typical Meteorological Year Version 3). Table 2.1 shows annual average irradiance, average temperature and wind speed. The relation between Global irradiance, Beam irradiance and diffuse irradiance is expressed as:

$$I_g = I_b cos(Z) + I_d \tag{2.1}$$

Where Z is the incidence angle,I_g is the global irradiance, I_b is the beam irradiance and I_d is the diffuse irradiance. Beam irradiance is usually more intense the Global because of the cosine losses. The equation does not consider ground reflected radiation.

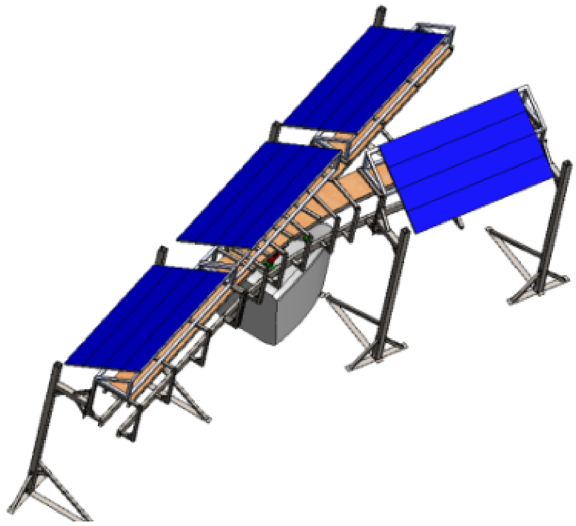

FIGURE 2.6: Design 1

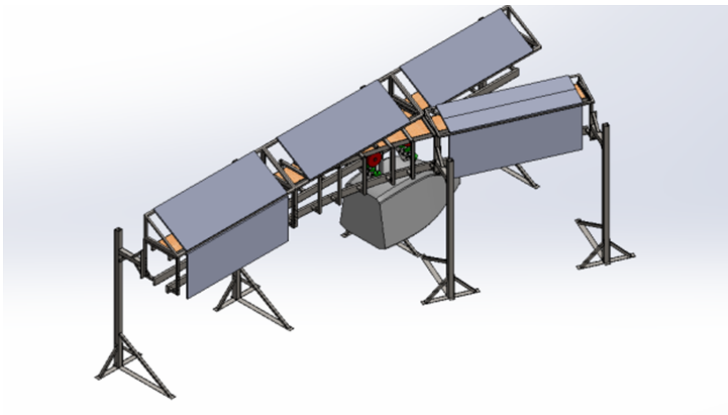

FIGURE 2.7: Design 2

2.4.2 Module

2.4.2.1 Solar array 1

Information about the modules used is presented in figure 2.12. Solar Array 1 used panels of the FLEX 02N type. The module performance data was extracted from the manufacturer datasheet. The Cell typeis CIGS (Copper, Indium, Galium and Selenium), one of the thin film module categories. These modules usually have efficiency between 7 and 14%, but are cheaper then panels of other types with greater efficiencies, because its manufacturing doesnt use expensive raw materials or high purity silicon wafers, unlike other kinds of modules, like polycrystalline silicon, for instance. All the electrical specifications were obtained from manufacturer‘s datasheet(TEAM, 2015a).

The maximum power point voltage, 32.5 V, is a reasonable value, because it is within the MPPT voltage range of operation for the chosen inverter, 30V to 50V. At the STC (Standard Test Conditions, which are 1000 W/m^2 of light intensity, radiation spectrum

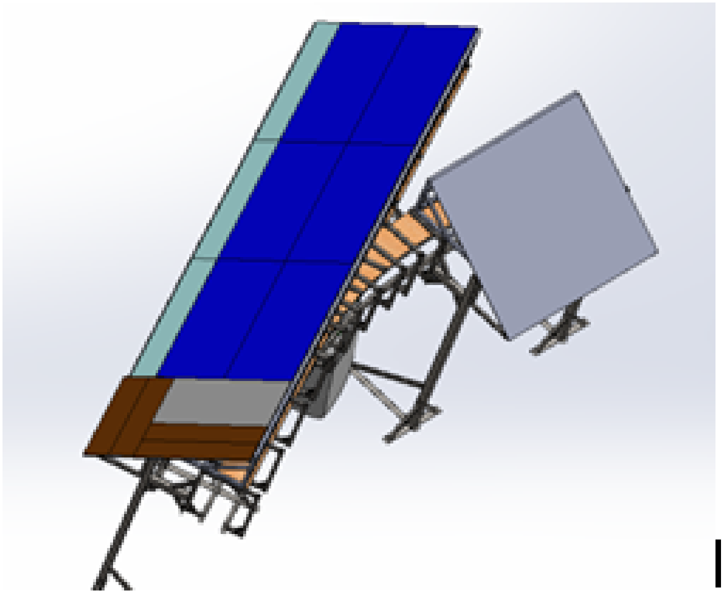

FIGURE 2.8: Design 3

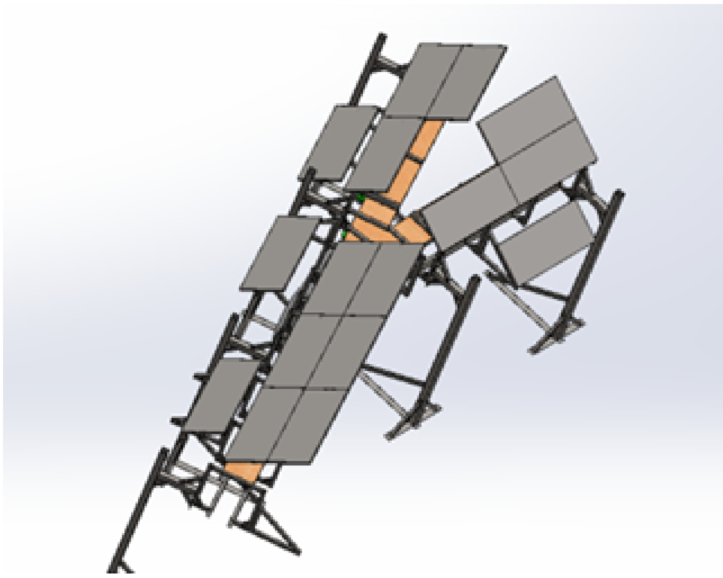

FIGURE 2.9: Design 4

similar to sunlight hitting the Earth‘s surface at latitude 35° North and 25 °C of cell temperature), the power is the product of MPPT current (4 A) and MPPT voltage (32.5 V), which gives the value of 130 Wdc. The efficiency of 13.5135% is a typical value for a CIGS cell type module. The solar energy-to-electricity conversion efficiency is calculated from data stored in a library of module parameters for thousands of commercially available modules. It is also an implementation of the single-diode equivalent circuit model described in the introduction.

The open circuit voltage (V_{oc}) and short circuit current (I_{sc}) are characteristic param-

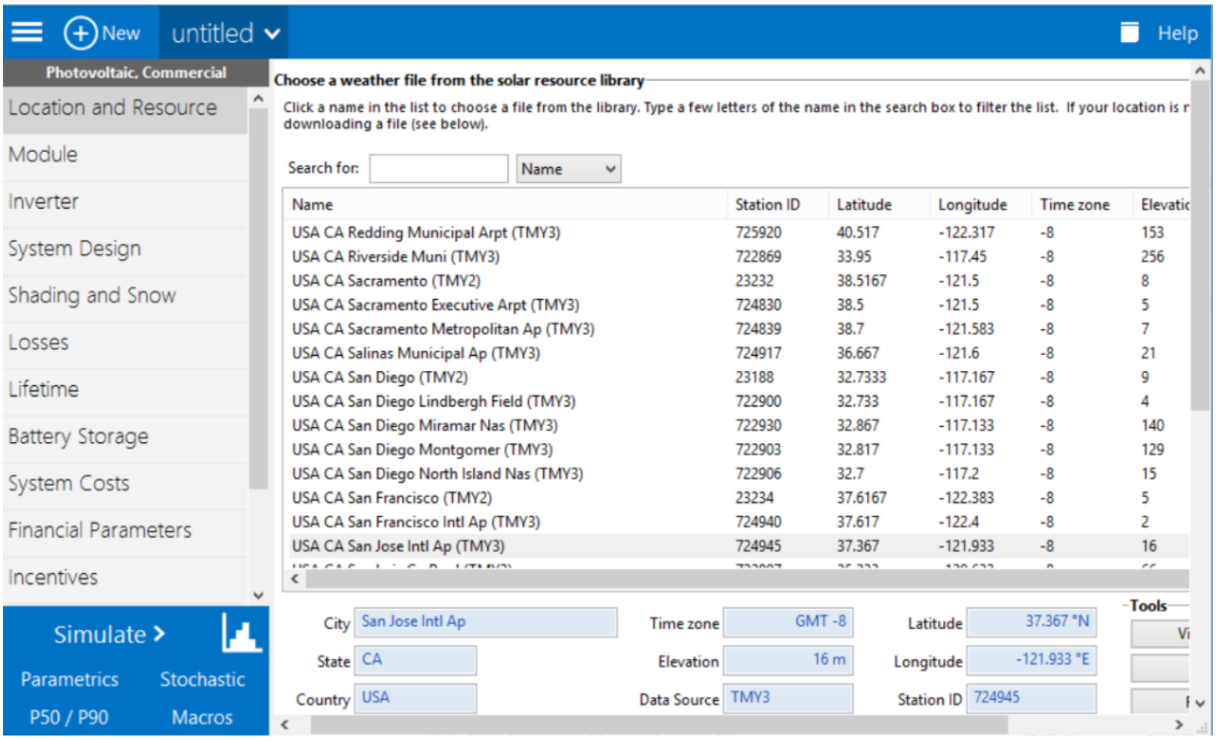

FIGURE 2.10: Initial interface of SAM

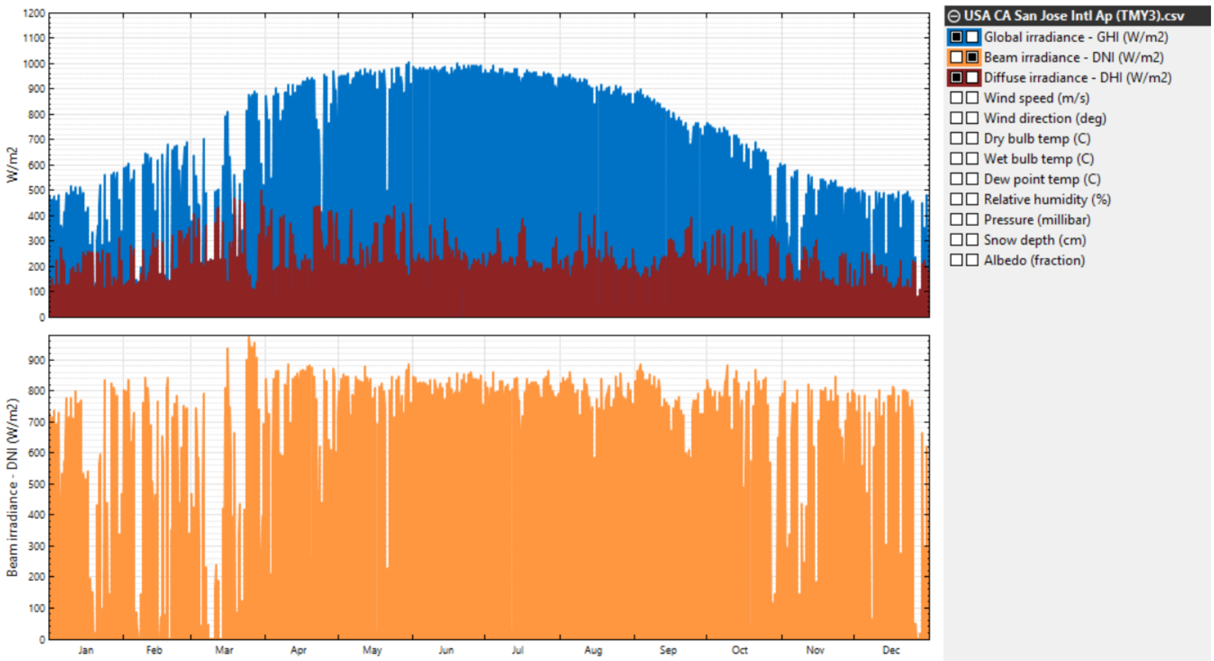

FIGURE 2.11: Initial interface of SAM Hourly Global, beam and diffuse irradiance in San Jose International Airport

eters of the module and are used to plot its I-V characteristic curve, like explained in the introduction. The I-V curve of the module in the right side of figure 16. The temperatures coefficients of V_{oc}, I_{sc} and maximum power point show how these parameters change with

TABLE 2.1: Annual irradiance, temperature and wind speed in San Jose International Airport

Parameter	Unit	Value
Average Global Irradiance	kWh/m^2/day	4.96
Average Beam Irradiance	kWh/m^2/day	5.35
Average Diffuse Irradiance	kWh/m^2/day	1.67
Average Wind Speed	m/s	3.0
Average Temperature	°C	14.9

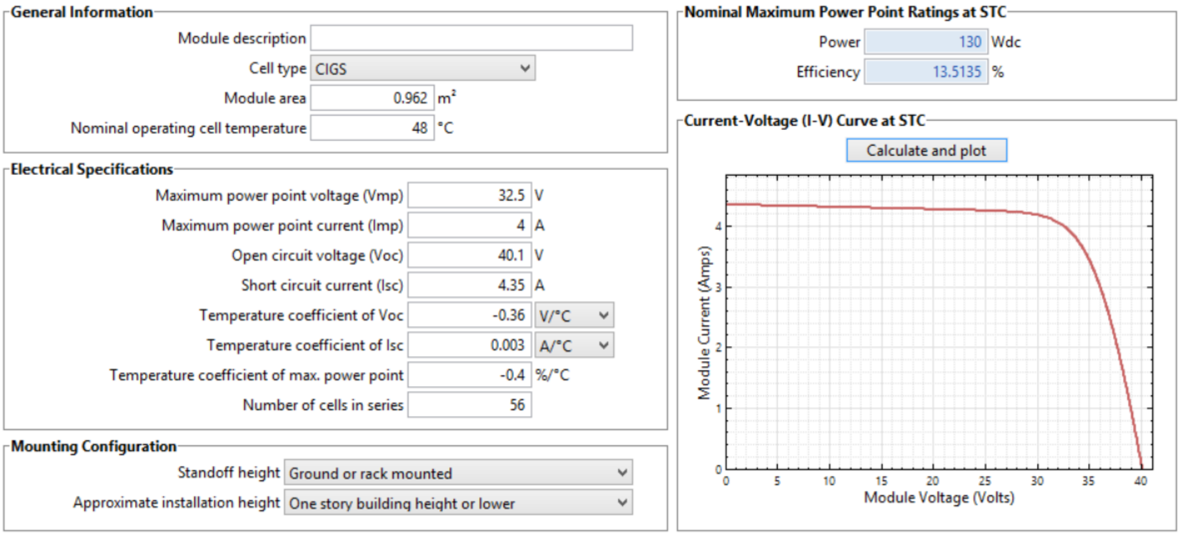

FIGURE 2.12: Solar Array 1: Module characteristics

variation of temperature. The modules were assumed rack mounted in one story building height or lower.

2.4.2.2 Solar array 2

Information about the modules used is presented in figure 2.13(TEAM, 2015b). Solar Array 2 used panels of the FLEX 02W type. At the STC, the power is the product current (11.33 A) and voltage (32.5 V), which gives the value of 351.23 Wdc. The efficiency of 13.5088% is a typical value for a CIGS cell type module.

2.4.3 System Design

For maximum power output, solar modules in the north hemisphere should face true south, which is different from magnetic south, the south pole of the Earth‘s magnetic field. So, it was assumed that the side of the guideway with more panels was facing south.

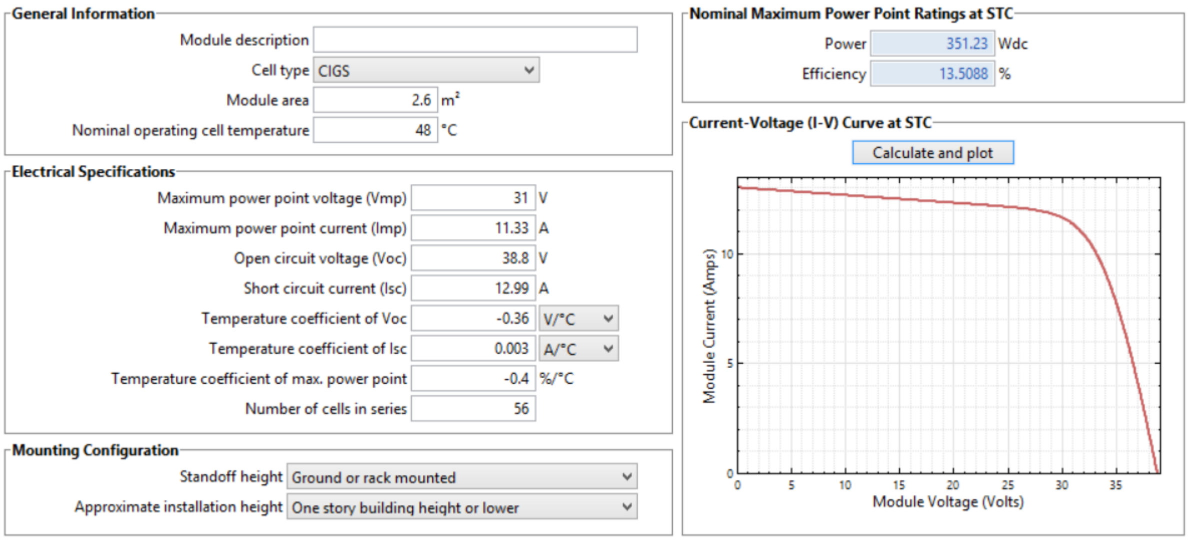

FIGURE 2.13: Solar Array 2: Module characteristics

These assumptions were made for all four configurations.

The system design consists of choosing specific characteristics for the arrays, like: how many modules in series per string and how many strings in parallel, number of inverters to be used and for each subarray, define azimuth and tilt angles. It is important to mention that the power outage of the circuit of solar panels is as greater as the current generated by the system, so to get the maximum power to the grid it is necessary to maximize this current, which can be done putting the modules in parallel (the total current is the sum of the currents generated by each module, and the total voltage is the same as of panels). Also, it was more convenient to work in low voltage values. In bigger systems, it is necessary to mount some strings of modules in series (which increases the total voltage), because usually there is a limit for the maximum current output into the grid or in a battery.

2.4.3.1 Solar Array 1

The first solar configuration consists of sixteen modules of the FLEX-02N type in a tilt angle of 31.22°. One side of the guideway contains 12 panels and the opposite site has the remaining 4. The angle between the tracks in the switching section of the guideway is 23.62°, like in figure 2.14. The system design consists of 2 subarrays, one of them with 12 modules at azimuth 180°, and the other one with 4 modules at azimuth 23.63°. Figure 2.15 gives information about the system design parameters.

The system is composed by 2 subarrays: one of them with 12 panels at azimuth 180° with tilt angle of 31.22°, and the other one with 4 panels at azimuth 23.62° with tilt angle

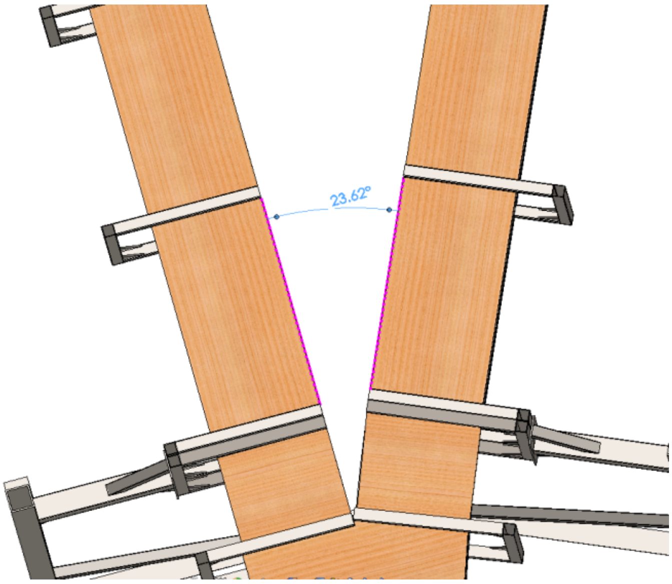

FIGURE 2.14: Angle between tracks

of 31.22°. All the panels are fixed to avoid costs in the development of a tracking system. The Ground Coverage ratio (GCR) is the ratio between the photovoltaic area and the ground area. It represents the spacing between rows of solar modules.

It was assumed that all the strings are in parallel so the string voltage would be 32.5 V and the current output would be maximum: 4 A per module, which results in the total of 64 A.

The number of inverters was 6 so it would result in a good DC to AC ratio, because the nameplate capacity (maximum power developed by the modules in the reference conditions) was 2080 kWdc and the maximum AC power for each inverter is 300 kW, so with 6 inverters the maximum AC power is 1800 kWac, which gives an DC to AC ratio of 1.16. The equations behind the calculated parameters are(NATIONAL..., 2015):

Module

- DC to AC ratio: ratio between total DC power generation and AC power output obtained from the inverter.

$$r = \frac{N_c}{C_i} 100\% \tag{2.2}$$

  Where r is the DC to AC ratio, N_c is the Total Nameplate Capacity in DC kW and C_i is the Total Inverter Nameplate Capacity in AC kW.

- Nameplate capacity (kWdc): The maximum DC power output of the array at the reference conditions.

$$N_c(kWdc) = M_{mp}(Wdc)(0.001kW/W)(n_m) \tag{2.3}$$

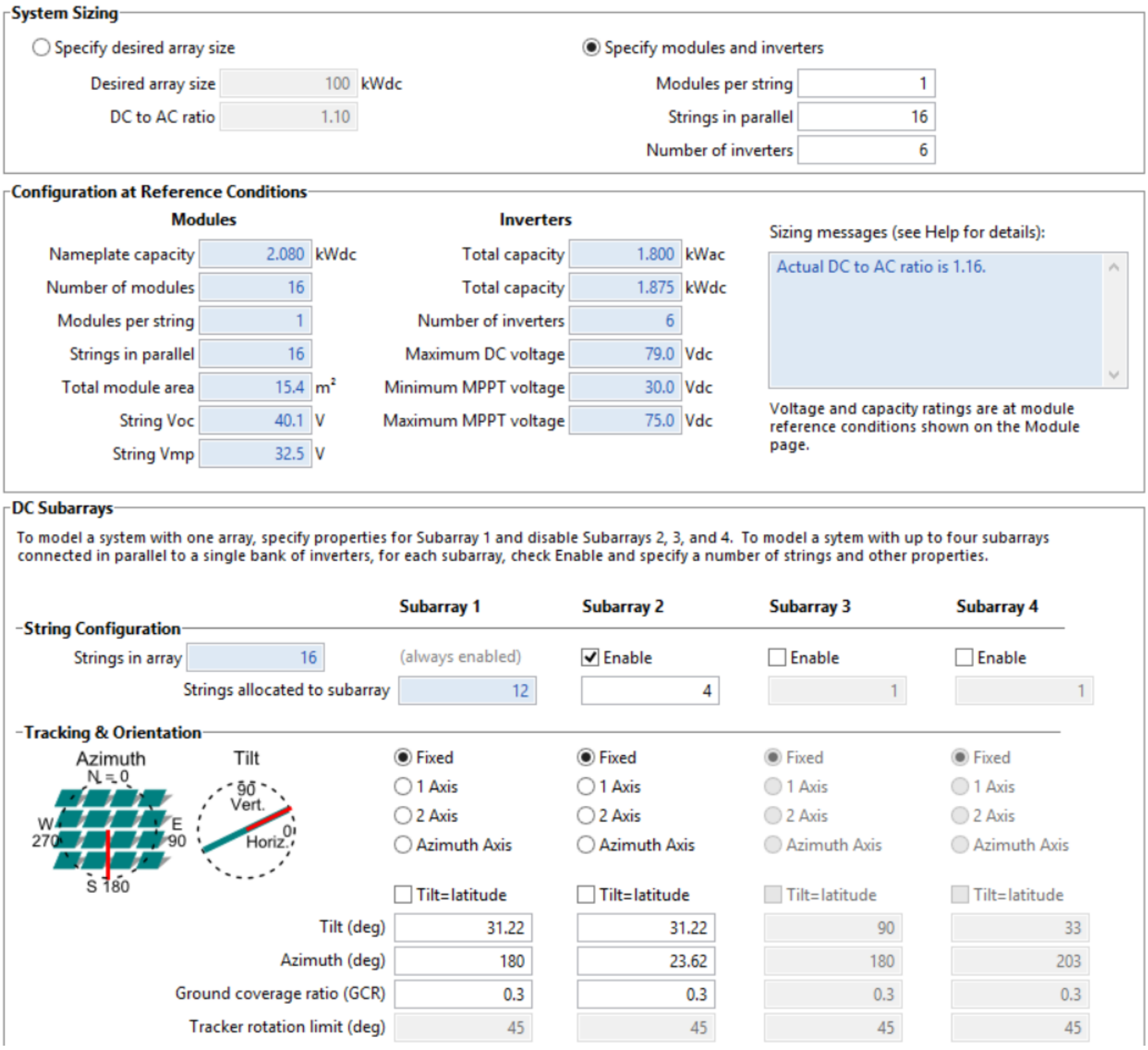

FIGURE 2.15: Solar Array 1: System Design

Where N_c is the nameplate capacity in kWdc, M_{mp} is the Module Maximum Power in Wdc and n_m is the number of modules.

- Total module area: The total area in square meters of modules in the array, not including space between modules.

$$A_t(m^2) = A_m(m^2)n_m \tag{2.4}$$

Where A_t is the total module area, M_{mp} is the Module Maximum Power in Wdc and n_m is the number of inverters.

- String V_{oc} (Vdc): The open circuit DC voltage of each string of modules at 1000

W/m^2 incident radiation and 25°C cell temperature.

$$V_{soc}(Vdc) = V_{oc}(Vdc)n_{ms} \tag{2.5}$$

Where V_{soc} is the string open circuit voltage, V_{oc} is the Module open circuit voltage and n_{ms} is the number of modules per string.

- String V_{mp} (Vdc): The maximum power point DC voltage of each string of modules at the module reference conditions shown on the module section.

$$V_{mp}(Vdc) = M_{mp}(Vdc)n_{ms} \tag{2.6}$$

Inverter

- Total capacity (kWac): The total inverter capacity in AC kilowatts.

$$I_{actc}(kWac) = I_{acmp}(0.001kW/W)n_i \tag{2.7}$$

Where I_{actc} is the inverter total capacity in kWac, I_{acmp} is the Inverter Maximum Power in Wac and n_i is the number of inverters.

- Total capacity (kWdc): The total inverter capacity in DC kilowatts.

$$I_{dctc}(kWdc) = I_{dcmp}(0.001kW/W)n_i \tag{2.8}$$

Where I_{dctc} is the inverter total capacity in kWdc, I_{dcmp} is the Inverter Maximum Power in Wdc and n_i is the number of inverters.

The other inverter parameters will be defined in the system inverter description.

2.4.3.2 Solar Array 2

The second solar configuration consists of four subarrays of FLEX-02W modules. One of them is consisted of three modules at azimuth 180° with tilt angle of 31.22°, other one consists of 1 module at azimuth 180° with tilt angle 90°, other one consists on one module at azimuth 203° with tilt angle 90° and the last one consists of one module at azimuth 203° with tilt angle 203°.Figure 2.16 gives information about the system design parameters:

The Tracking and Orientation section in figure 2.16 shows the four subarrays described previously. The panel in Subarray 2 is almost flat so it won‘t shade the modules located behind it, the ones on top of the structure that are tilted 31.22°.

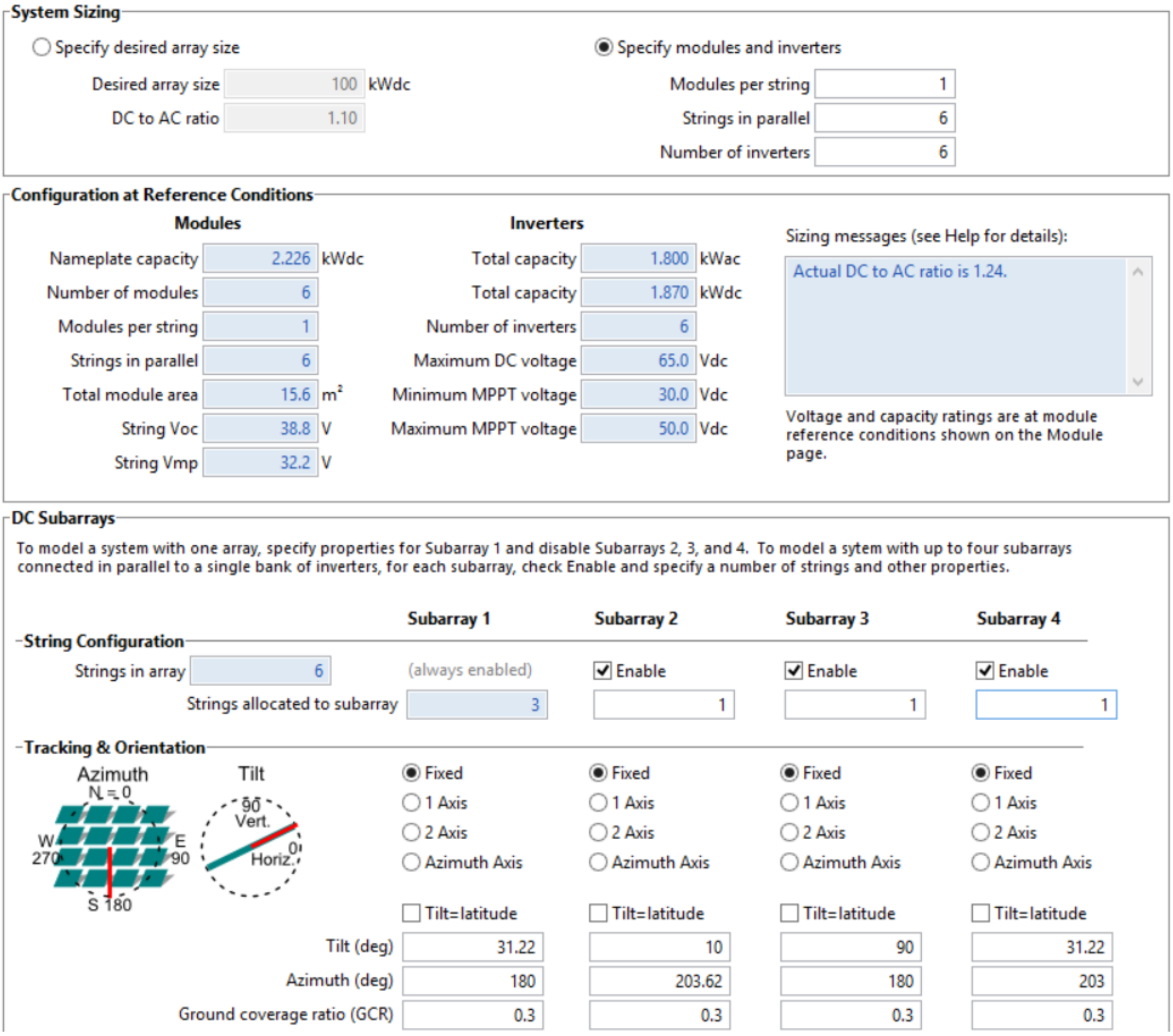

FIGURE 2.16: Solar Array 2: System design parameters

It was assumed that all the strings are in parallel so the string voltage would be 31 V and the current output would be maximum: 11.33 A per module, which results in the total of 67.98 A.

The number of inverters was 6 so it would result in a good DC to AC ratio, because the nameplate capacity (maximum power developed by the modules in the reference conditions) was 2107 kWdc and the maximum AC power for each inverter is 300 kW, so with 6 inverter the maximum AC power is 1800 kWac, which gives an DC to AC ratio of 1.17.

2.4.4 Inverter

The function of the inverter is to convert DC power from PV modules into AC power to the grid or to AC loads. SAM has a database of available electrical inverters to be chosen for a given solar energy collection system. The inverter ABB MICRO-0.3-I-OUTD-

US-208 208V was chosen from the database. Figure 2.17 gives information about the used inverter.

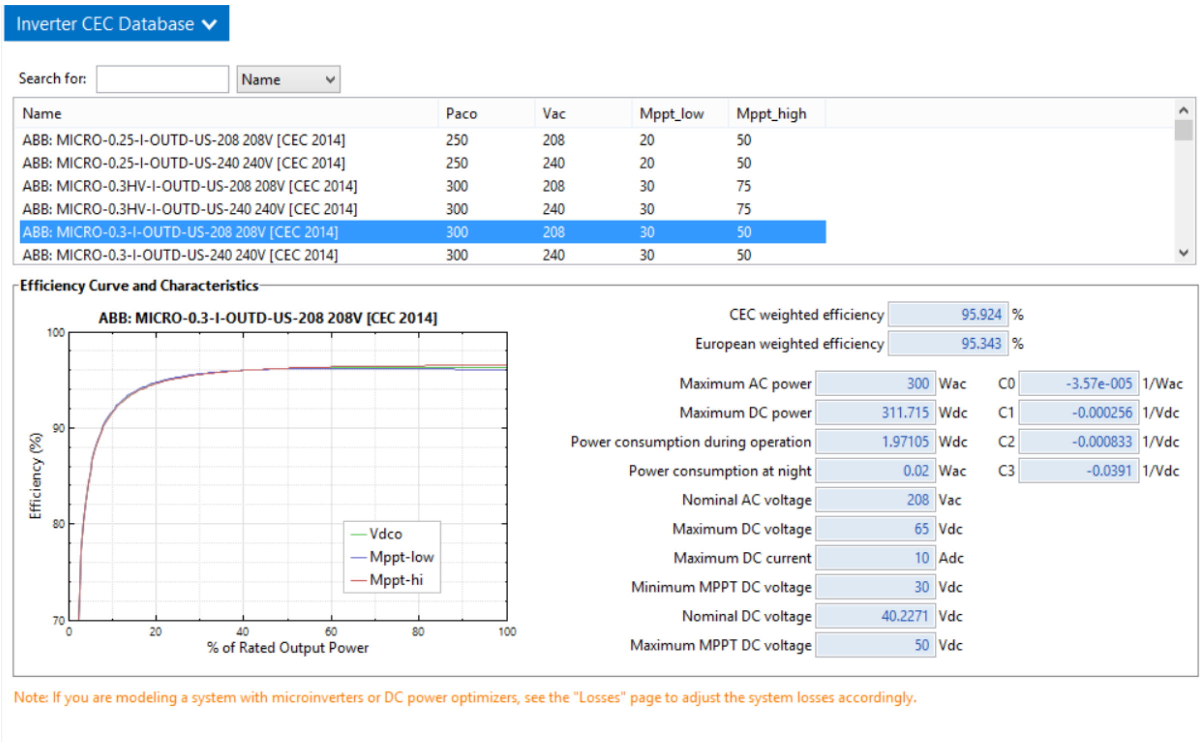

FIGURE 2.17: Datasheet of the chosen inverter.

The European weighted efficiency is an averaged operating efficiency over a yearly power distribution in European weather conditions. It was proposed by the Joint Research Center (JCR/Ispra), based on Ispra (Italy) weather . It can be obtained by the following equation(EUROPEAN..., 2014):

$$Euro_{eff} = 0.03Eff_{5\%} + 0.06Eff_{10\%} + 0.13Eff_{20\%} + 0.1Eff_{30\%} + 0.48Eff_{50\%} + 0.2Eff_{100\%} \tag{2.9}$$

Where $Eff_{x\%}$ is the efficiency at x % of nominal power. Like shown above, the European weighted efficiency for the chosen inverter is 95.343%. For climates of higher insolations, like United States South-West, the California Energy Commission has proposed another weighting, specified for inverters used in US(EUROPEAN..., 2014):

$$CEC_{eff} = 0.04Eff_{10\%} + 0.05Eff_{20\%} + 0.12Eff_{30\%} + 0.21Eff_{50\%} + 0.53Eff_{75\%} + 0.05Eff_{100\%} \tag{2.10}$$

Like shown above, the CEC efficiency for the chosen inverter is 95.924%. This inverter has the efficiency of 95.924%, with minimum MPPT DC voltage of 30 V and maximum MPPT DC voltage of 50 V, which is a range that contains most of the available modules output DC voltage. The characteristics shown in CEC Database model are available from manufacturer specifications. They are(NATIONAL..., 2015):

- Maximum AC power (P_{aco}): Maximum AC power output at nominal operating conditions;

- Maximum DC power (P_{dco}): Input DC power lever at which the AC power output is maximum;

  These two parameters are related by the following equation:

$$P_{dco} = P_{aco}/eff \tag{2.11}$$

  Where eff is the conversion efficiency.

- Power Consumption during operation (P_{so}): DC power required to start conversion process. It is not always available in manufacturer‘s specifications, so it can be estimated by 1% pf the inverter‘s maximum AC power.

- Power Consumption at night (P_{nt}): AC power consumed by inverter at night when the PV array is not generating power.

- Nominal AC voltage (V_{ac}): Rated output AC voltage.

- Maximum DC voltage (V_{dcmax}) and Maximum DC current (I_{dcmax}): Inverter‘s maximum DC input voltage and maximum voltage input at or near PV array‘s maximum power point current.

- Maximum DC voltage (V_{dcmax}) and Maximum DC current (I_{dcmax}): Inverter‘s maximum DC input voltage and maximum current input, typically at or near PV array‘s maximum power point current.

- Minimum MPPT DC voltage ($MPPT_{low}$) and Maximum MPPT DC voltage ($MPPT_{high}$)): Respectively, minimum and maximum DC operating voltage, determined empirically in CEC test protocol, which specifies that the inverter‘s maximum DC voltage should not exceed 80% of the array‘s maximum open circuit voltage.

- Nominal DC voltage (V_{dco}): The mean between $MPPT_{low}$ and $MPPT_{high}$, also described by CEC test protocol.

The efficiency curve shown on the right of figure 9 is a performance model provided by the CEC test protocol by measuring performance (efficiency) at six different power levels

(10%, 20%, 30%, 50%, 75% and 100% of ac-power rating)(KING SIGIFREDO GONZALES, 2007) and three different voltage levels ($MPPT_{low}$, $MPPT_{low}$ and V_{dco}) and modelling the results by the following equations(NATIONAL..., 2015):

$$P_{ac} = \{\frac{P_{aco}}{A-B} - C(A-B)\}(P_{dc} - B) + C.(P_{dc} - B)^2 \tag{2.12}$$

$$A = P_{dco}\{1 + C_1(V_{dc} - V_{dco})\} \tag{2.13}$$

$$B = P_{so}\{1 + C_2(V_{dc} - V_{dco})\} \tag{2.14}$$

$$C = C_0\{1 + C_3(V_{dc} - V_{dco})\} \tag{2.15}$$

The four coefficients C_0, C_1, C_2 and C_3 are empirically-determined coefficients that are inputs to the Sandia inverter model. C_0 defines the relationship AC and DC power levels at the reference operating conditions, C_1 defines the value of the maximum DC power level, C_2 defines the value of self-consumption power level and C_3 defines the value of Coefficient C_0. P_{ac} and P_{dc} are respectively AC and DC power at a given operation point(KING SIGIFREDO GONZALES, 2007).

A MPPT (maximum power point tracking) is an electronic device that controls the operating point to optimize the match between solar systems and the battery or utility grid. The charge controller compares the output of the panels and the battery voltage to estimate the best power and voltage conditions to maximize the current into the battery. The inverter in use has the interval of 30V to 50V to the MPPT DC voltage.

This inverter was chosen because of its good performance characteristics, and because the maximum power point voltage of both modules used are inside the range between $MPPT_{low}$ and $MPPT_{high}$.

Inverter clipping losses could occur if the inverter AC power output exceeds the inverter nameplate AC capacity or the Array's voltage falls outside the range between minimum and maximum MPPT limits. In the first case, Sam adjusts the output to the inverter nameplate capacity, and in the second case, SAM adjusts the array voltage to the minimum or maximum MPPT voltages(NATIONAL..., 2015).

2.4.5 Shading and Snow

To simplify the models of the solar systems, it was not considered shading or snow losses in any of the analysis.

2.4.6 Losses

The overall losses assumed of the models were the ones assumed in figure 2.18.The first section shows losses in the DC part of the system. It was applied to all subarrays of the PV systems. Soiling losses reduce solar radiation incident in subarray. SAM calculates the incident radiation from its weather files and array angle and subtract the soling loss from it. The losses in the circuit caused by mismatch (difference of performance between modules in array), diodes and connections (voltage drops across blocking diodes and electrical connections), DC wiring (resistive losses on the wiring on the DC side of the system) and nameplate (accuracy of the manufacturer‘s nameplate rating, often caused by degradation of the modules when exposed to light) can be seen above. The model did not consider tracking error (inaccuracies in tracking mechanism) and DC optimizer losses (power losses for additional power conditioning equipment installed with the array). The total DC power loss was calculated by equation 2.16 and total DC power output is expressed by equation 2.17:

$$P_{ldc} = 1 - [(1 - L_m)(1 - L_{dc})(1 - L_{dcw})(1 - L_{te})(1 - L_n)(1 - L_{dco})] \tag{2.16}$$

Where P_{ldc} is total DC power loss, L_m is loss by mismatch, L_{dc} is loss by Diodes and connections, L_{dcw} is loss by DC wiring, L_{te} is loss by tracking error, L_n is loss by nameplate and L_{dco} is DC power optimizer loss.

$$P_{dc} = \sum_{i=1}^{n} P_{dci}(1 - P_{ldci}) \tag{2.17}$$

Where n is the number of subarrays, P_{dc} is Net DC array power, P_{dci} is subarray i gross DC power and P_{dcli} is subarray i total DC power loss.

The second section of figure 2.18 shows losses in the AC side of the system. SAM applies total AC loss and reduce inverter AC output. The two sources of losses are AC wiring (electrical losses in AC wiring between the inverter and the grid connection point) and step-up transformer (transformer electrical losses). The model only considered for AC wiring losses. The total AC power loss was calculated by the following equation 2.18 and the total AC power output is expressed in equation 2.19:

$$P_{lac} = 100\%[1 - (1 - L_{acw} \div 100\%)(1 - L_{sut} \div 100\%)] \tag{2.18}$$

Where P_{adc} is total AC power loss, L_{acw} is loss by AC wiring and L_{sut} is step up transformer loss.

$$P_{ac} = P_{aci}(1 - P_{laci}) \tag{2.19}$$

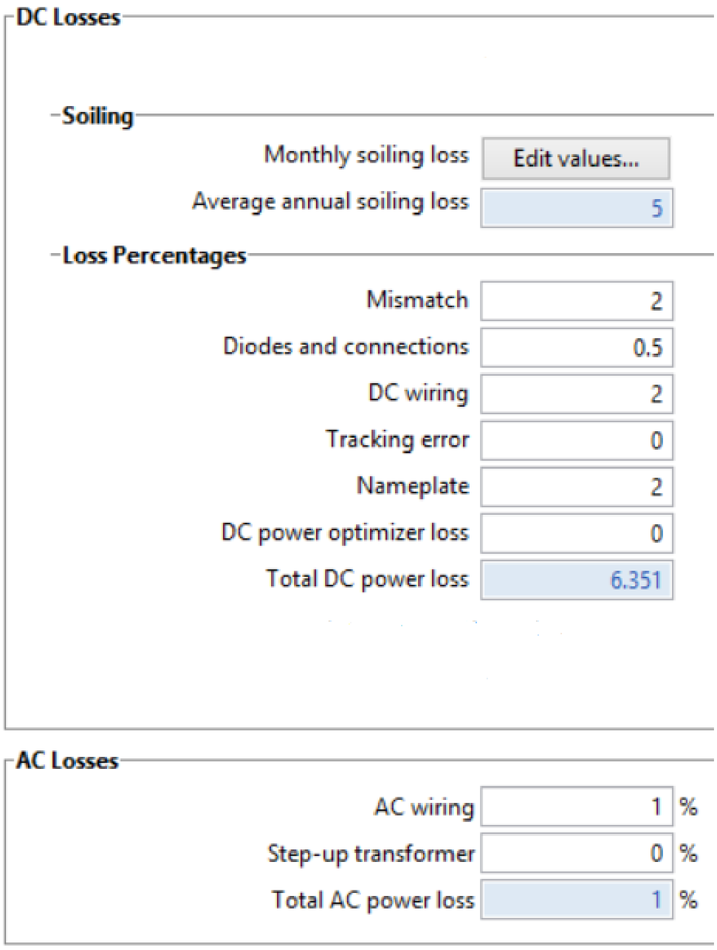

FIGURE 2.18: Losses Assumptions.

Where P_{ac} is Net AC array power, P_{aci} is subarray i gross AC power and P_{laci} is subarray i total AC power loss.

2.4.7 Lifetime Degradation

The performance of a solar array decreases over the years, and in SAM model there is an estimate rate to the degradation, which was assumed to be of 0.5% per year.

2.4.8 Battery Storage

The prototype that should run with photovoltaic energy is supposed to work at night as well, where the PV panels are not collecting energy to be input in the bogie to move it. Therefore, the system side should include a battery to store energy to be used in the prototype during this period. If the battery energy is not enough to make the system work at night, it would be necessary to purchase energy from the grid.

2.4.8.1 Solar Array 1

Figure 2.19 shows initial configurations for the battery bank in Solar Array 1. A rechargeable battery cell is consisted of material setup responsible for a chemical reaction that can produce current to a specific load if it occurs in one way and store energy if it occurs in the opposite way, which can be forced by moving current in the way opposite to the spontaneous direction. These are called, respectively, the processes of discharge and charge of a battery. There are several types of battery cells that use different chemical mechanisms to store energy. The process of charge and discharge of a battery is called a cycle.

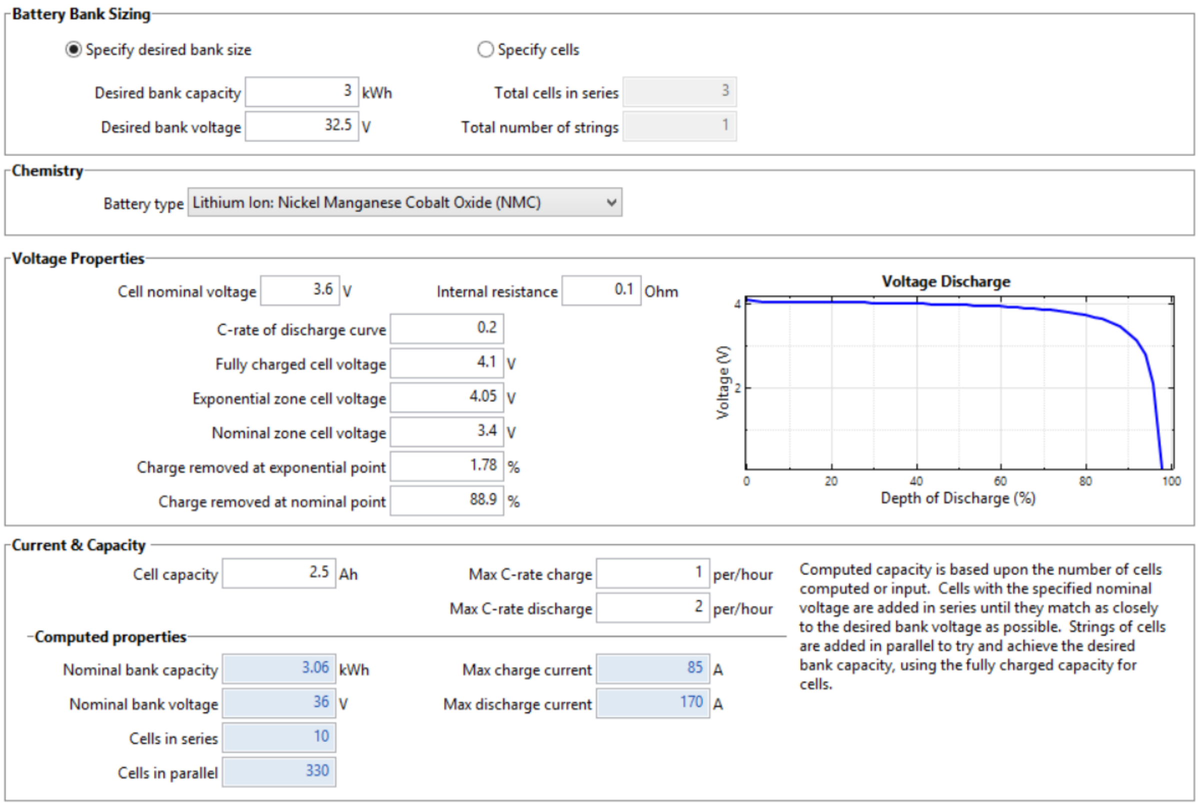

FIGURE 2.19: Battery Configurations for Solar Array 1: Battery Bank Sizing Chemistry, Voltage Properties, Current and Capacity, Power Converters.

The capacity of storage of the battery decreases with the increase of the number of cycles that the battery does. The Battery bank is a group of battery cells connected in parallel or in series in order to increase the bank voltage and current. The total energy storage capacity is 3 kWh and the chosen bank voltage is 32.5 V to work in the closer voltage as possible to the modules MPPT voltage. SAM calculates the approximate necessary number of cells in parallel and in series based in these inputs. The equations used by the software to calculate it are 2.20 and 2.21:

$$V_b = V_c n_{cs} \tag{2.20}$$

$$C_b = V_c c_c n_{cp} \tag{2.21}$$

Where V_b is bank voltage, V_c is cell nominal voltage, n_{cs} is the number of cells in series, c_c is cell capacity, C_b is bank capacity and n_{cp} is the number of cells in parallel.

The type of cell used was the Lithium-Ion Battery NMC (Nickel Manganese Cobalt Oxide), more specific the LG Model ICR18650 B4 2600 mAh(LEE, 2010). This type of cell is relatively cheap compared to other types of Lithium Ion batteries and also cells of the lead acid type. This type of chemistry has better safety characteristics as well. The data present in the Voltage properties section was extracted from the manufacturers datasheet. SAM plots a Voltage Discharge curve based on this information. This curve is consisted of two regions, the nominal zone, where the voltage is approximately constant with time, and the exponential zone in the beginning of the discharge process, before entering the nominal zone. Figure 2.20 shows the curve with its characteristic regions:

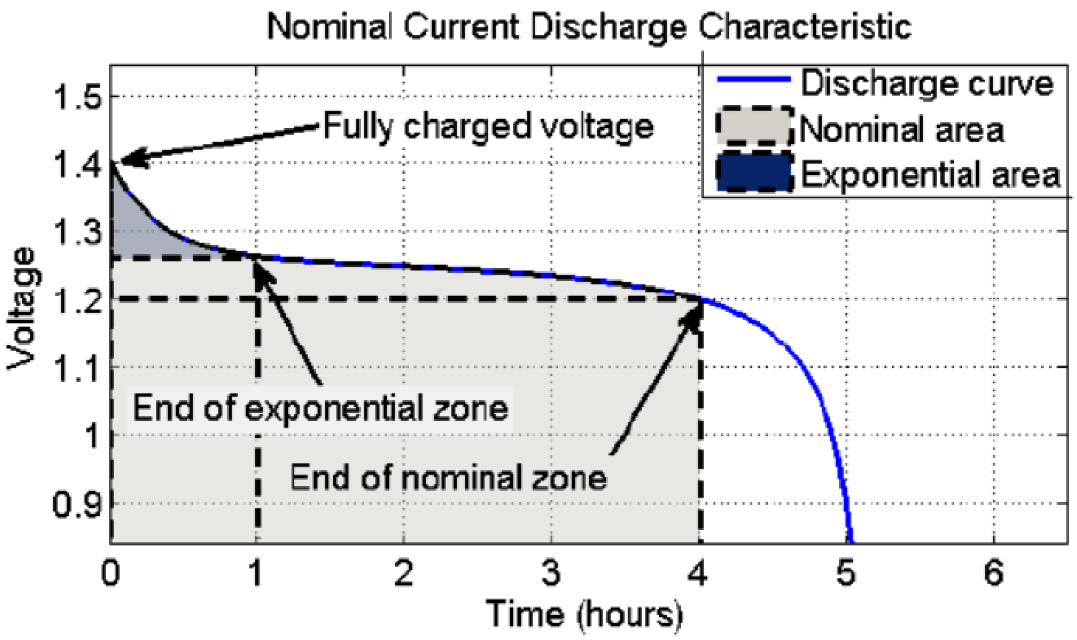

FIGURE 2.20: Nominal Current Discharge Characteristic.

The cell nominal voltage in the voltage for a given type of cell, and usually it is around 3.7 volts for Lithium-Ion cells and around 2V for Lead-Acid cells. The cells have an internal resistance of 0.1 ohms. The C-rate of discharge is a parameter to define the current used to discharge the battery, expressed as the current divided by the rated capacity, and it is 0.2 for the cell of this case. The other parameters of the Voltage properties are points of the Discharge Curve that SAM uses to plot it(NATIONAL..., 2015). The Current Capacity Section gives information about the bank capacity of energy storage, which is 3.024 kWh, the bank voltage, which is 50.4 V, the cell capacity of charge, which is 2.5 Ah and the maximum C- rates of charge and discharge are respectively 1 per/hour and 2 per/hour(LEE, 2010). Equations 2.22 and 2.23 relate the maximum charge and discharge currents with the desired bank capacity, the bank voltage, and the C-rates of charge and discharge, respectively. It was assumed that both AC to DC and DC to AC energy conversion are 99

$$I_{maxc} = \frac{C_b(kWh)}{V_b(V)} \times (1000Wh/1kWh) \times C_{rate_{cmax}}(per/hour) \tag{2.22}$$

$$I_{maxd} = \frac{C_b(kWh)}{V_b(V)} \times (1000Wh/1kWh) \times C_{rate_{dmax}}(per/hour) \tag{2.23}$$

Where I_{maxc} is the maximum charge current, $C - rate_{cmax}$ is maximum C-rate of charge, I_{maxd} is the maximum discharge current and $C - rate_{dmax}$ maximum C-rate of discharge.

The desired cell capacity is 3kWh and the desired bank voltage is 48 V, the maximum C-rate of charge is 1 per/hour and the maximum C-rate of discharge is 2 per/ hour, so, according to equations 2.24 and 2.25, the maximum current of charge is approximately 60 A and the maximum current of discharge is approximately 120 A.

Figure 2.21 shows the sections of Manual Storage Dispatch Controller, where is defined how the battery will be charged from the grid or from the PV system and how it will discharge, and Battery Lifetime, that shows how the effective capacity decreases with the number of discharge cycles.

The battery was configured to discharge during night (approximately from 7 PM to 6 AM), in periods 1 and 3, and to be charged from the PV system when daylight is available (approximately from 7 AM to 6 PM), in period 2. When the option Allow discharging is enabled, it is necessary to specify how much of the battery‘s available charge the system can dispatch by inputting a capacity to discharge. This value will be hourly dispatched from the available charge if the battery is allowed to discharge. The available charge is defined by the minimum state of charge and the maximum state of charge. The capacity of charge is 25% (the battery will go from the maximum state of charge to the minimum state of charge in four hourly periods), so it would be necessary to charge the battery from the grid to keep it working all night. This is the reason why charging from the grid was allowed in period 1.

The Battery Lifetime Section shows one lifetime tests made to study the capacity

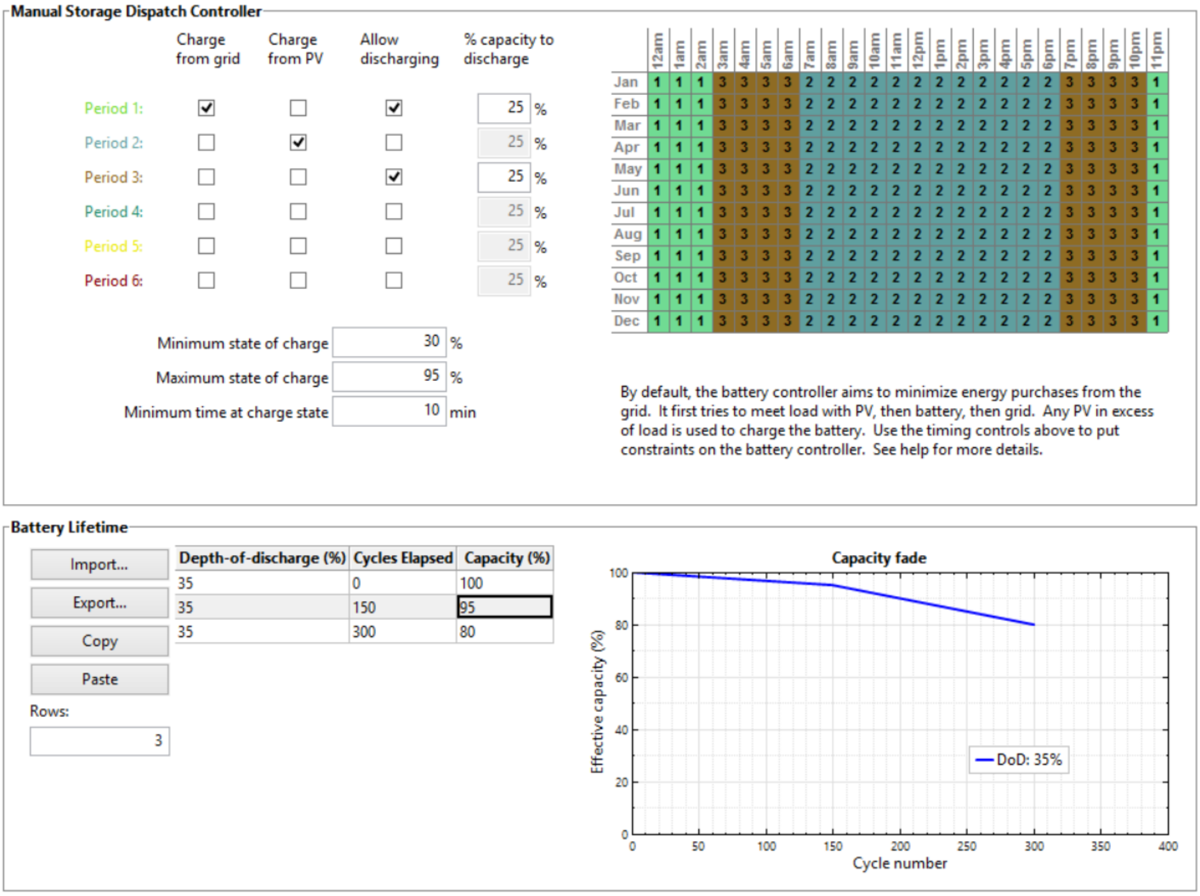

FIGURE 2.21: Battery Configurations: Manual Storage Dispatch Controller and Battery Lifetime.

decrease with number of cycles. The blue curve shows that, with a depth of discharge of 35%, the cell loses 20% of its initial capacity in 300 cycles. This information was obtained from the manufacturer‘s datasheet(LEE, 2010). Figure 2.22 shows battery replacement configurations and thermal properties. It is necessary to replace battery periodically due to degradation caused by cycling. It was chosen to replace the battery when it reaches 20% of its original capacity. Actually, the cost of energy generated by Lithium Ion NMC batteries in the market is approximately $400.00/kWh, and the escalation of the cost was assumed to be equal to inflation. The information about thermal properties was extracted from the manufacturer‘s datasheet. The curve on the right shows dependence of discharge capacity with operating temperature. Cp is the specific heat of the battery, which was assumed to be 1004 kJ/kgK, and h is the heat transfer coefficient between the battery and the environment, which was assumed to be 1004 kJ/kgK. The designed battery has a specific energy per mass of 187.5 Wh/kg and a specif energy per volume of 517Wh/L.

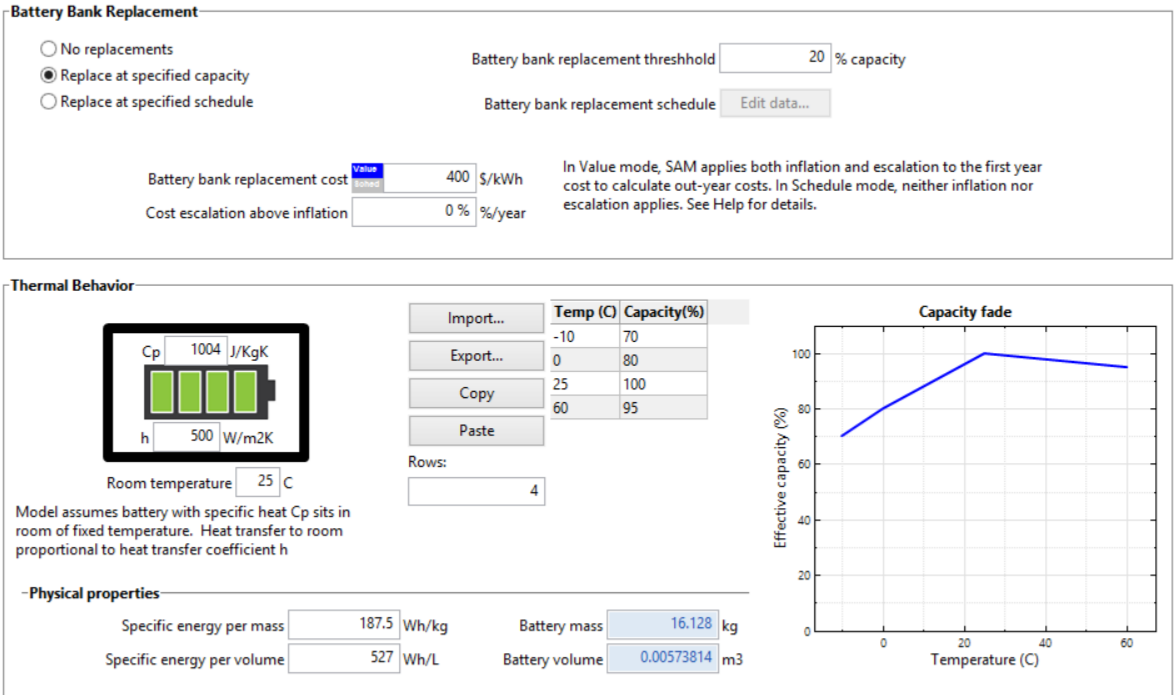

FIGURE 2.22: Battery Bank Replacement and Thermal Behavior.

2.4.8.2 Solar Array 2

The battery bank configurations for Solar Array 2 are almost the same as the Solar Array 1. The only differences are the Battery Bank Sizing and Voltage Properties sections, because the battery bank voltage now is 32.2 V to get as close as possible to the MPPT voltage of the FLEX-02 W Modules. This changes the number of cells in parallel and in series necessary to attend the conditions of voltage and capacity. These sections of Solar Array are shown in Figure 2.23.

2.4.9 System Costs

For the system costs, only the direct capital costs were considered. In Solar Array 1, from the modules datasheet, there is a costs of 1.03 $/Wdc for each solar panel, and a good average value for the inverter cost is 1.00 $/Wac. Costs with the energy storage were considered as well. Like said before, there is a cost of $400.00/kWh DC to store energy using Lithium Ion NMC batteries. The remaining system costs are shown in figure 2.24.

Contingency is a percentage of the total direct cost that can be accounted for expected uncertainties in direct cost estimates.

The equipment necessary to install the equipment would be the materials to do the racking and the backing, clamps to attach the modules to the support and bolts to keep the

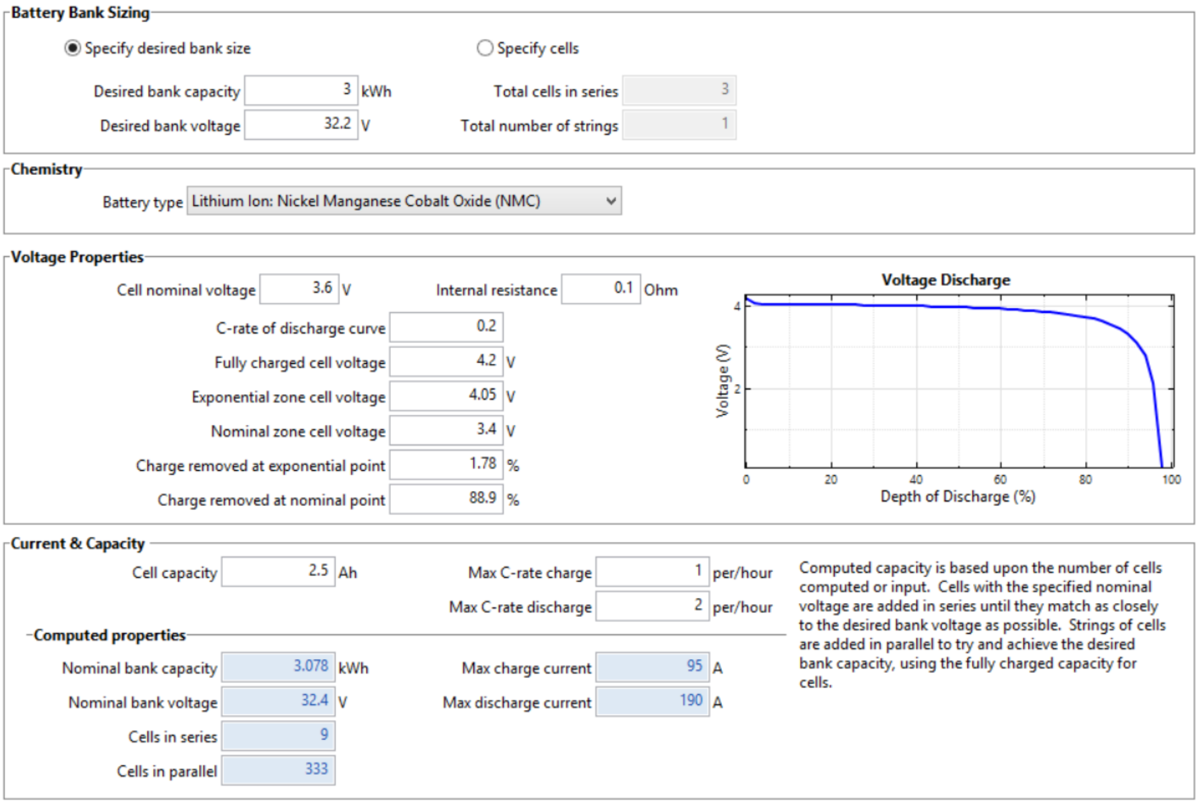

FIGURE 2.23: Battery Configurations for Solar Array 2: Battery Bank Sizing, Chemistry, Voltage Properties, Current and Capacity, Power Converters.

parts together with the structure. The shop where the project was being developed already had some materials that would be used in the racking, which decreased the equipment costs. The costs with the installer (installation labor and Installer margin and overhead) are not very high, considering that this is a small solar system, only to generate power for the bogie in the full scale model. It can be observed that solar array

2.4.10 Financial Parameters

Figure 2.25 shows financial parameters assumed for the Commercial Financial model. The debt fraction is the percentage of the net capital cost that would be financed by loan. The loan term is the number of years required to pay the loan and the loan rate is the annual nominal interest rate of for the loan. The currently model did not assume any loan payment to be input in the project, so all these parameters are zero. The net capital cost is equal to the total installed cost from the System Costs page less any cash incentives (capacity based incentives or investment based incentives), which were not applied for the model as well. The Weighted Average Cost of Capital (WACC) is defined as the minimum return that the project must earn to cover financing costs. SAM calculates it as defined in equation 2.24(NATIONAL..., 2015):

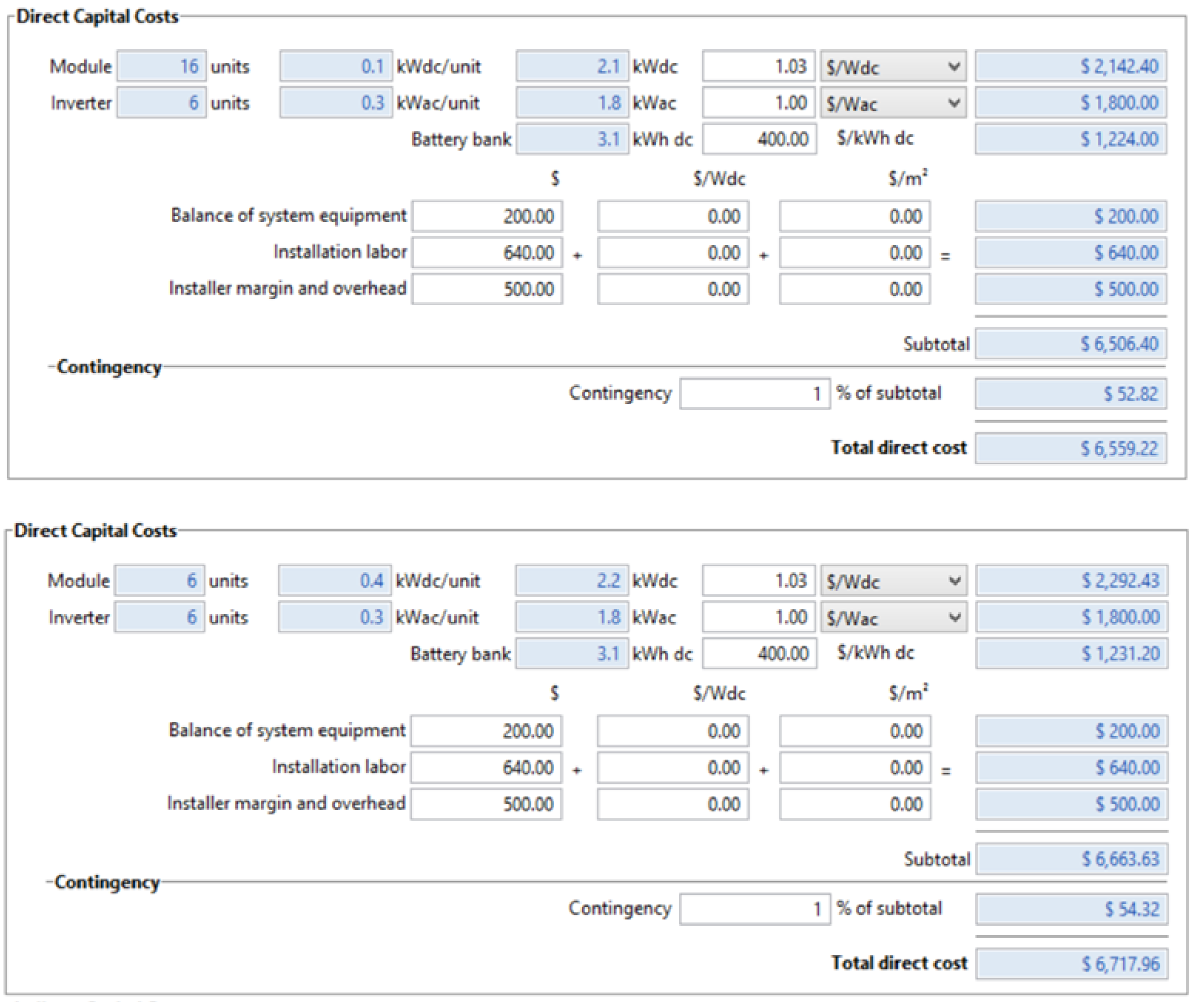

FIGURE 2.24: System costs for Solar Array 1 on the top and for Solar Array 2 on the bottom.

$$WACC = d_{real} \times (100\% - d_f) + (100\% - e) \times l \times d_f \tag{2.24}$$

Where d_{real} is the real discount rate, d_f is the debt fraction, e is the effective rate and l is the loan rate. The effective tax rate accounts for both state tax income and federal tax income and is calculated as:

$$e = f_t \times (100\% - s_t) + s_t \tag{2.25}$$

Nominal discount ratio is calculated by the followinf equation:

$$d_{nominal} = (1 + d_{real})(1 + i_r) - 1 \tag{2.26}$$

Where f_t is federal Tax Rate, s_t is State Tax Rate,$d_{nominal}$ is the nominal discount

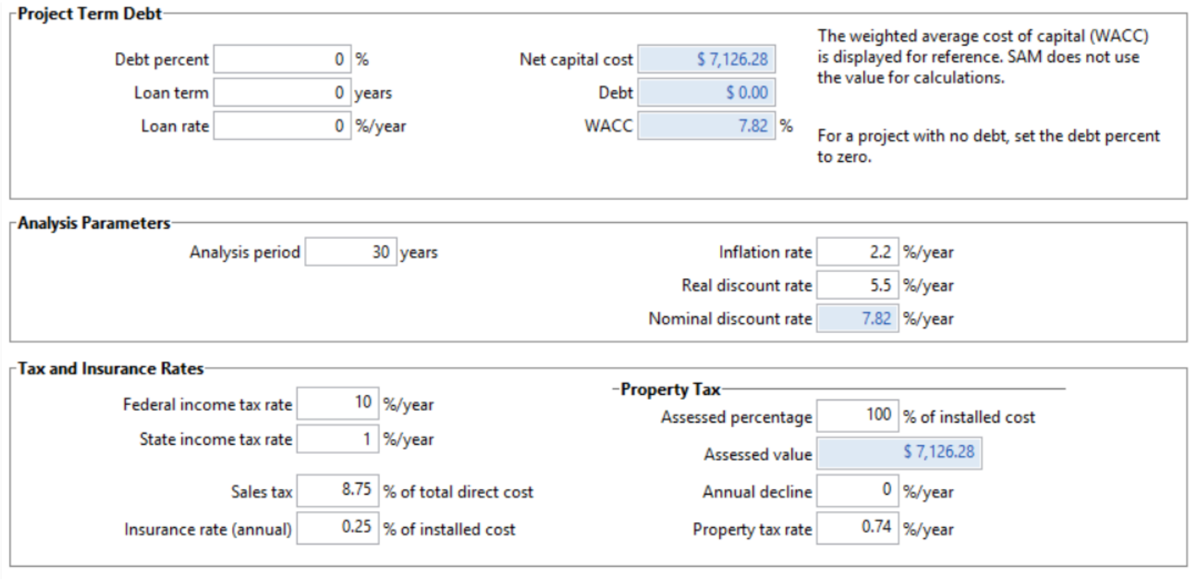

FIGURE 2.25: Financial parameters.

TABLE 2.2: United States Federal Income Tax Rate

Taxable Income Range	Federal Tax Rate(%)
Between \$0 and \$9225.00	10
Between \$9225.00 and \$37450.00	15
Between \$37450.00 and \$90750.00	25
Between \$90750.00 and \$189300.00	28
Between \$189300.00 and \$411500.00	33
Between \$411500.00 and \$413200.00	35
More than \$413200.00	39.6

rate, d_{real} is the real discount rate and i_r is the inflation rate . The values for the inflation rate (annual rate of change of costs), real discount rate (time value of money expressed as an annual rate), federal and state income tax rates (tax benefits and liabilities), sales tax (tax for the sale of goods and services), insurance rate (annual insurance payment)(SPEER MICHAEL MENDELSOHN, 2010) and property tax rate were assumed according to the economical characteristics of San Jose, California in the first semester of 2015. Federal(FEDERAL..., 2015) and State tax rates depend on the net capital cost of the project, which is \$7126.28. This dependence can be verified on tables 2.2 and 2.3. The property tax is the main source of revenue for local governments, and it is calculated as the fair market value of the property times an assessment ratio (which is 100% for this analysis) times a tax rate (which is 0.74% for California(CALIFORNIA..., 2015)). The assessment ratio can have an annual decline rate, but it was considered constant for this model. The analysis period of 30 years was chosen to allow an analysis for a time greater than the payback period.

TABLE 2.3: California State Income Tax Rate

Taxable Income Range	State Tax Rate(%)
Between \$0 and \$7168.00	1
Between \$7169.00 and \$16994.00	2
Between \$16995.00 and \$26821.00	4
Between \$26822.00 and \$37223.00	6
Between \$37234.00 and \$47055.00	8
Between \$47056.00 and \$1000000.00	9.3
More than \$1000000.00	10.3

2.4.11 Incentives

For all projects, incomes from any incentives are taxable, but for residential and commercial projects, SAM does not apply taxes to the value of electricity saved by the system. For commercial projects like this one, SAM reduces the project cash flow by the amount of federal and state income tax on the value of the electricity, because the savings represent the value of electricity purchases that would have been a tax-deductible operating expense to the commercial entity.

To develop a solar system in USA, it is important to look for federal and state incentives that could financially help in the project development. SAM suggests the DSIRE (Database of State Incentives for Renewables and Efficiency) website to look for policies and Incentives.

In the state of California, the following policies and incentives were assumed to be applied for the project:

Property Tax Exclusion for Solar Energy Systems: It is a state implemented property tax incentive that offers 75% of system value exemption for this case of power generation system. For this model, it was considered a maximum amount of \$4000.00 incentive. Other eligible technologies are Solar Water Heat, Solar Thermal Electric and Solar Thermal Process Heat(PROPERTY..., 2014).

Business Energy Investment Tax Credit (ITC): It is a federal implemented corporate tax credit program that claims a credit of 30% of expenditures for solar systems. It also offers incentives for fuel cells, microturbines, small wind turbines and other technologies. It was considered a maximum amount of \$4000.00 incentive for this model too(BUSINESS..., 2015).

2.4.12 Electricity Rate

The electricity rate determines how the system owner will be financially compensated by the energy generated. For commercial financial models, the electricity generates offsets purchases of electricity to meet the ATN load. Figure 2.26 shows the assumptions made for the electricity rate:

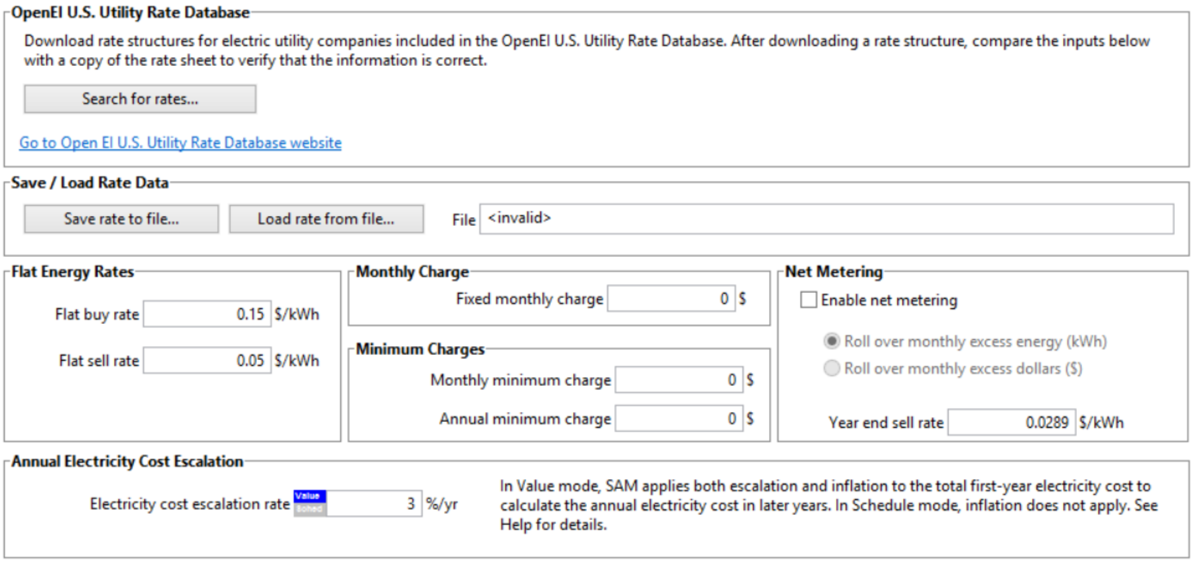

FIGURE 2.26: Electricity Rate.

For disabled net metering, every month that the produced energy is less than the load, electricity will be bought at the flat buy rate, which for this case is 0.15$/kWh and if the opposite happens, electricity will be sold at the flat sell rate, which for this case is 0.05$/kWh.

For enabled net metering, there is no sell rate, because every month that the systems produces more electricity than the monthly load, there is a credit in kWh or dollar to the next month electricity bill, and credit at the end of the year are established at the year-end sell rate.

Like shown above, the analysis did not enable net metering, so there is a sell rate. The electricity cost escalation rate shows how the electricity price increases from year to year.

2.4.13 Electric Load

The load of the system is the power necessary to move the bogie in the prototype. Development of the prototype model is more concerned with cost and simplicity than performance. The speed is to be fast enough to allow onlookers to observe its operation, while also being slow enough to prevent collisions with objects or people and reduce the

TABLE 2.4: Assumed conditions for prototype

Parameters	Value	Units	BOE
Vehicle Weight	250	Kg	T
Nominal Speed	1	ft/sec	D
Maximum Acceleration	1	ft/sec^2	D
Traction Force Max	115	N	A
Peak Torque	11.637	Nm	A
Continuous Torque	3.9172	Nm	A
Revolutions Per Minute	28.648	Rpm	D
Peak Power	34.911	W	A
Continuous Power	11.752	W	A
Normal Force	164	N	A

cost of components. The assumed conditions and performance requirements are summarized below. The monthly load is 20.95 kWh then, considering that the podcar is always moving(TEAM, 2015).

BOE means Basis of Estimate. It is T for tested parameter, D for design specification and A for analytically estimated parameter. The table shows that the average power consumed for bogie propulsion is 11.752 W. So, multiplying it for 24 hours per day times the number of for each month, it results in the load shown in figure 2.27.

The monthly energy showed in figure 2.27 is a result of the assumption of an average load power of 11.752 W. SAM works with time steps and calculate the total energy used in a month by summing all the products between the time steps and the load power in the respective time step. To do this, it is necessary to input an hourly load data. In this case, there is no load data available, only the monthly energy usage, but SAM comes with a set of computer-generated hourly data for some cities in the United States, like San Jose for instance.

In this model, the option Normalize supplied load profile to monthly utility bill data was enabled. It permits working with monthly electric usage data in SAM, because the software scales the hourly data in the computer-generated hourly load data to match the monthly usage data. For instance, if the monthly usage is 1000 kWh and the monthly usage in the load data is 1500 kWh (a ratio of 1.5) SAM divides all the hourly load power in the respective month by 1.5. The peak scaled load power value in each month is shown in Figure 14. Figure 2.28 shows a comparison between the hourly load data from SAM database, named here user entered load data, and the scale load data(NATIONAL..., 2015).

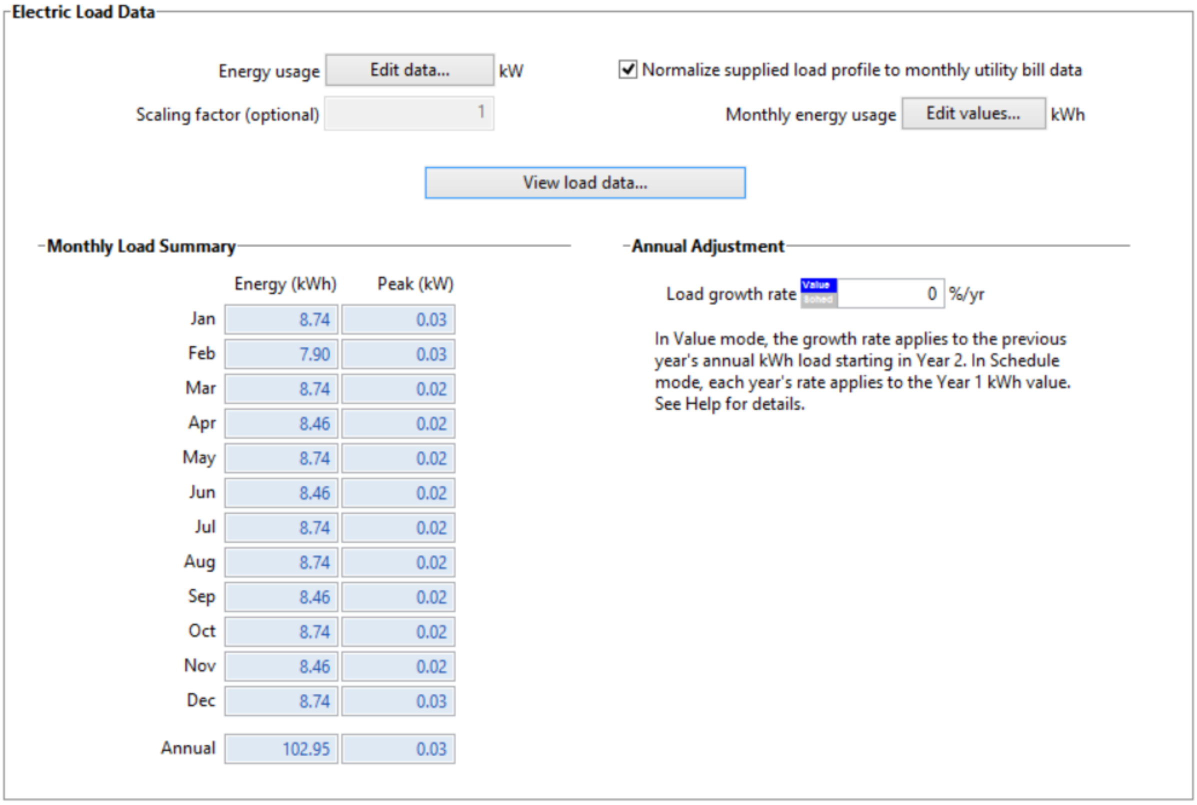

FIGURE 2.27: Annual Electric Load.

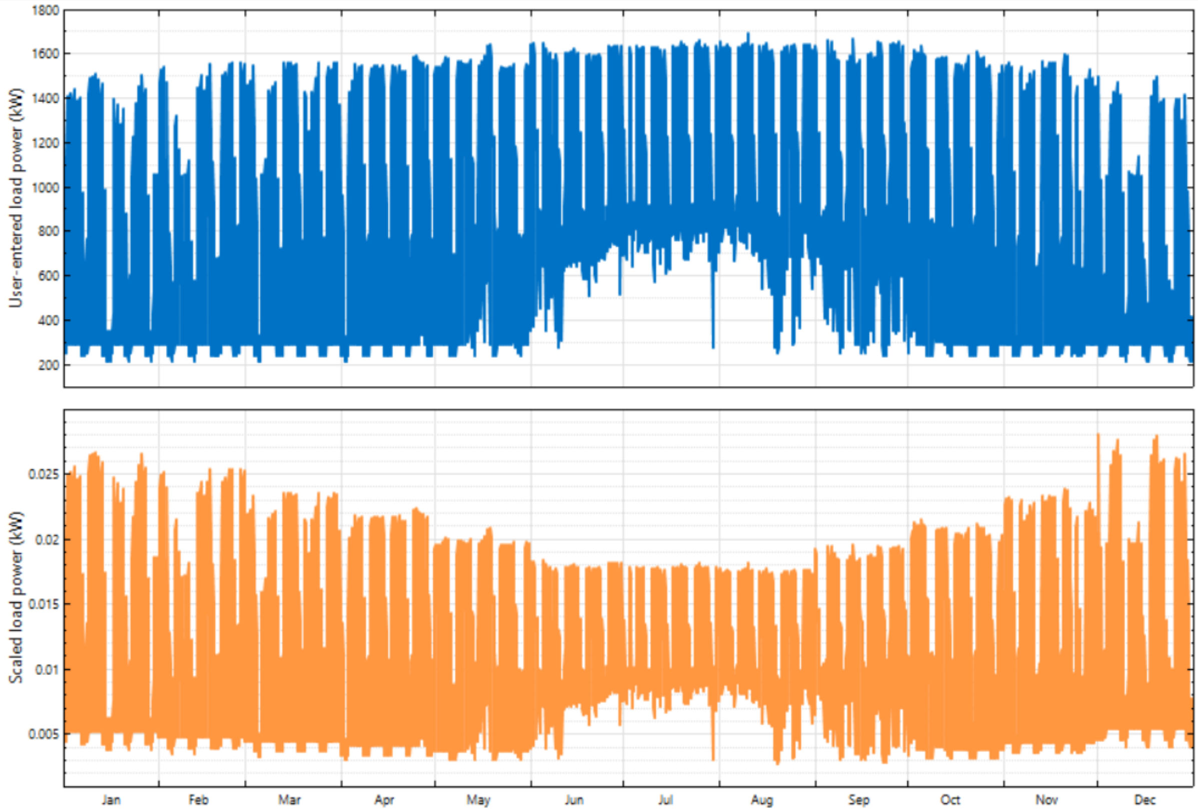

FIGURE 2.28: User-entered load power (kW) and Scale load power (kW).

3 Results

The summary of the results obtained for the simulations are presented in tables 3.1 and 3.2.

The annual energy shows that this is a small solar system, which is coherent with the goal of supplying the full scale model of the Spartan Superway. SAM shows annual energy for the first year of the project cash flow. It calculates it by multiplying irradiance from weather files by the computed efficiencies for each of the subarrays and the time steps and summing all the energy parcels(NATIONAL..., 2015). The irradiance in a tilted surface is calculated by SAM using the consideration in figure 3.1 and the following equations(GOSWAMI *et al.*, 2000):

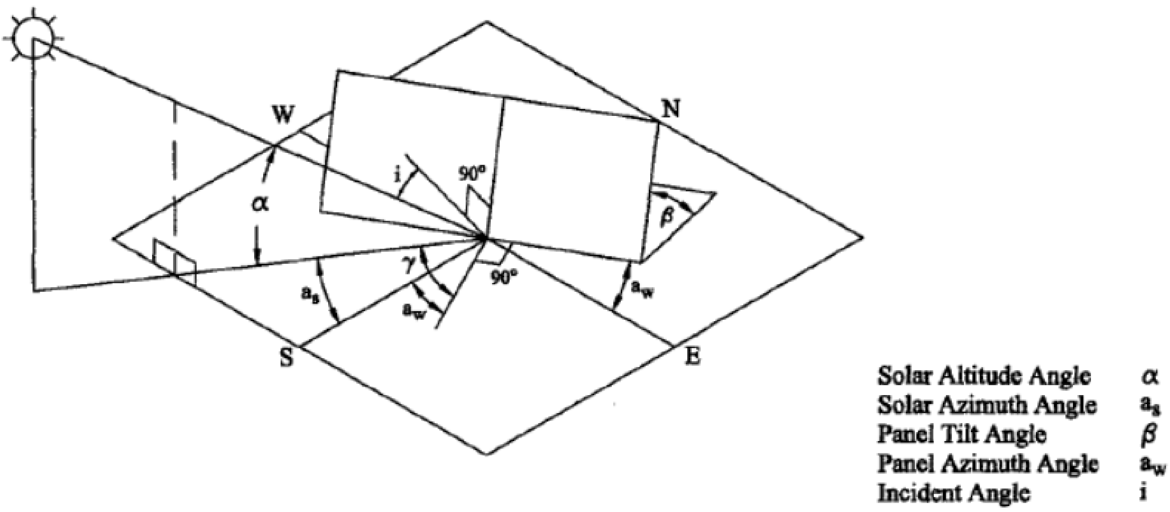

FIGURE 3.1: Parameters for irradiance calculation on a tilted surface.

$$I_c = I_{bc} + I_{dc} + I_{rc} \tag{3.1}$$

$$I_{bc} = I_{bN} cosi = I_{bN} cos(\alpha)cos(a_s - a_w)sin(\beta) + sin(\alpha)cos(\beta) \tag{3.2}$$

$$I_{dc} = CI_{bN}(cos(\beta/2))^2 \tag{3.3}$$

TABLE 3.1: Performance and financial parameters for Solar array 1

Metric	Unit	Value
Annual energy	kW	3014.00
Capacity factor	%	16.5
First year kWhAC/kWDC	kWh/kW	1449.00
Performance ratio	1	0.78
Levelized COE (nominal)	cents/kWh	6.35
Levelized COE (real)	cents/kWh	5.05
Electricity cost without system	$	28.00
Electricity cost with system	$	-122.00
Net savings with system	$	151.00
Net present value	$	414.00
Payback period	years	9.4
Net Capital cost	$	6559.00
Equity	$	6559.00
Debt	$	0

TABLE 3.2: Performance and financial parameters for Solar array 2

Metric	Unit	Value
Annual energy	kW	3300.00
Capacity factor	%	16.9
First year kWhAC/kWDC	kWh/kW	1483.00
Performance ratio	1	0.78
Levelized COE (nominal)	cents/kWh	6.18
Levelized COE (real)	cents/kWh	4.90
Electricity cost without system	$	28.00
Electricity cost with system	$	-137.00
Net savings with system	$	165.00
Net present value	$	520.00
Payback period	years	9.3
Net Capital cost	$	6718.00
Equity	$	6718.00
Debt	$	0

TABLE 3.3: Average values of sky diffuse factor (C) for 21^{st} day of each month, for average atmospheric conditions at sea level for the United States.

Month	C
1	0.058
2	0.060
3	0.071
4	0.097
5	0.121
6	0.134
7	0.136
8	0.122
9	0.092
10	0.073
11	0.063
12	0.057

$$I_{rc} = (\rho)I_{bN}(sin\alpha + C)(sin(\beta/2))^2 \tag{3.4}$$

Where I_{bc} is beam radiation, I_{dc} is diffuse radiation, I_{rc} is ground reflected radiation, I_c is global radiation, I_{bN} is beam radiation on a horizontal surface, C is the sky diffuse factor, which is defined in table 3.3, and ρ is a reflection coefficient that depends on the ground consistence. It is approximately 0.2 for ground or grass, and 0.8 for snow covered surface.

Some of the annual energy meets the electric load and some is sold to the grid at the retail rates. The capacity factor is the ratio between the annual energy produced and the amount of energy that would be produced if the system worked in its full nameplate capacity. For photovoltaic systems, it is usually below 25%.

$$C_f = (E_{annual}(kWhac/yr)/C_s)/8760(h/yr) \tag{3.5}$$

Where C_f is the capacity factor, E_{annual} is the net annual energy and C_s is the system capacity(NATIONAL..., 2015). The result obtained for this parameter is not so good, but it satisfies the necessities for this project. It shows that the system design could be made in other ways to improve the solar irradiation catching efficiency. The first year KWhac/kWdc is the ratio between the system‘s annual AC output in Year one to it‘s nameplate DC capacity.

$$r_1(kWhac/kWdc) = E_{annual}/N_c \tag{3.6}$$

Where r_1f is first year kWhac/kWdc , E_{annual} is the net annual energy and N_c is the system capacity. The performance ratio represents the relationship between the actual and theoretical energy output of the PV plant, showing the proportion that is available for export to the grid. It is calculated be deducing the losses that were showed in the losses section. High-performance PV plants can reach a performance ratio up to 80%.

$$PR = E_{annual}/E_{nominal} \tag{3.7}$$

Where PR is the performance ratio, E_{annual} is the net annual energy and $E_{nominal}$ is the nominal plant output in kWh(NATIONAL..., 2015).

Levelized Cost of Energy (LCOE) is the overall cost of installing and operating a project in dollars per kilowatt hour of electricity during its lifecycle. The calculation of this parameter includes all the costs over its lifetime: initial investment, operations and maintenance, and others. Another definition for it is the price per unit of energy that causes the investment to just break even. There are several ways to estimate it.

SAM evaluates the data showing the nominal LCOE and the real LCOE. The first one is a constant dollar, inflation-adjusted value, and the second one is a current dollar value(NATIONAL..., 2015). The value of Real LCOE is less than the nominal LCOE whenever the inflation rate is greater the zero, because the nominal discount rate used to compute the nominal LCOE includes inflation, it is factored out of nominal LCOE evaluation. The inflation rate in the analysis conducted is 2.2% per year, which explains why the nominal LCOE is greater than real LCOE. For commercial models, SAM assumes that the renewable energy system meets all or part of a building‘s electric load, so the levelized cost is comparable to a $/kWh retail electricity rate representing costs to meet the system load by purchasing electricity from the grid. To be economically viable, the project‘s LCOE must be equal or less than the average retail electric rate. Real and nominal LCOE are calculated by SAM using the following equations:

$$LCOE(real) = \frac{-C_0 - \frac{\sum_{n=1}^{N} c_n}{(1-d_{nominal})^n}}{\frac{\sum_{n=1}^{N} Q_n}{(1-d_{real})^2}} \tag{3.8}$$

$$LCOE(nominal) = \frac{-C_0 - \frac{\sum_{n=1}^{N} c_n}{(1-d_{nominal})^n}}{\frac{\sum_{n=1}^{N} Q_n}{(1-d_{nominal})^2}} \tag{3.9}$$

Where:

- Q_n is the electricity generated by the system in year n;
- N is the analysis period in years;
- C_0 is the project equity investment amount (the amount invested by the project owner or investor);
- C_n is the annual project costs in Year n;
- d_{real} is the real discount rate. It‘s the discount rate without inflation;
- $d_{nominal}$ is the nominal discount rate. It‘s the discount rate with inflation.

The values obtained for both types of LCOE are low, because of the low cost for the small solar system and the two incentives that were assumed in this analysis. The values of the real LCOE were very close to the flat sell rate, which means that the project is economically viable if inflation is not considered. SAM calculates electricity costs without the system by multiplying the system total load by the cost of the kWh in the project location, and the electricity cost with the system is calculated by subtracting the total energy produced by the system from the load and multiplying by the cost of the kWh. The net savings with system were not too high, but the payback period of approximately 9 years is less than the average value for solar systems (usually it is around 15 years), because of the incentives assumed. SAM considers the value of electricity generated by the system, tax benefits, and incentives to be project savings. Payback period is the time in years that it takes for the project savings to equal the net capital cost.

The project net present value (NPV) measures the project‘s feasibility account for both revenue and costs. A positive NPV indicates an economically feasible project. It is the present value of the after cash flow discount to year one using nominal discount rate. It can be expressed by the following equation:

$$NPV = \sum_{n=0}^{N} \frac{c_n}{(1 + d_{nominal})^n} \tag{3.10}$$

Where C_n is the after-tax cash flow in Year n, N is the analysis period in years and $d_{nominal}$ is the nominal discount rate. For both solar arrays, the positive net present value indicates an economically feasible project. Figure 3.2 compares monthly energy production between solar arrays 1 and 2. SAM calculates Monthly energy production by the same way that it calculates annual energy production.

Figure 3.2 above shows how energy production varies during the year. In the summer, the amount of energy produced increases by 100% because of the higher solar radiation. Figure 3.3 shows the degradation of the system during the years, according to the chosen degradation rate of 0.5

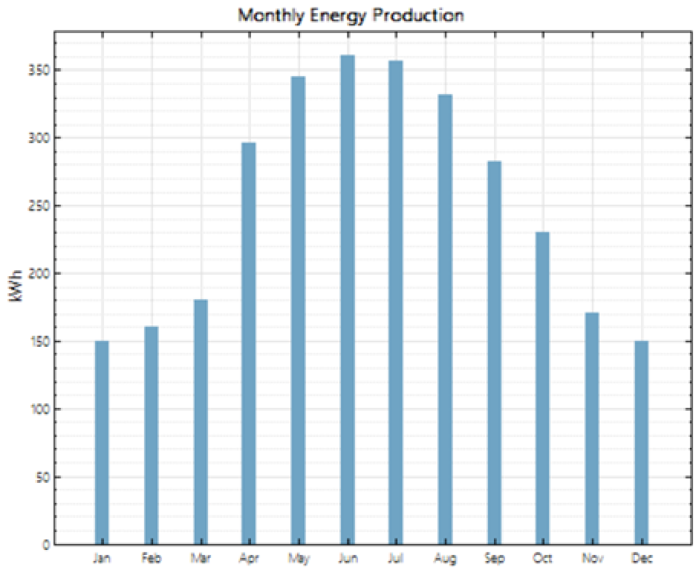

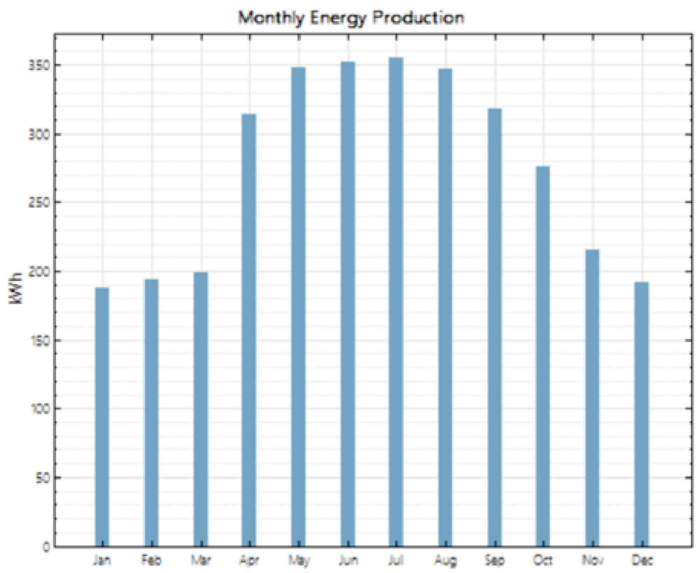

FIGURE 3.2: Monthly Energy production for Solar Array 1 (top) and Solar Array 2 (bottom).

Figure 3.4 shows after tax-cash flow for Solar Arrays 1 and 2 in the analysis period. In the first year, the total installed cost and the incentives come into play, and then there are yearly savings with electricity production. Table 3.3 show yearly savings for solar arrays 1 and 2.

The incentives are almost equal to the system costs in month zero, and the positive cash flow along the years contributes to a low payback period. The net present value is the difference between the cash inflow and the cash outflow by the end of the analysis period, and the positive value shows that the system is generating profit by the end of year.

Figure 3.5 compares monthly energy production with monthly load for both solar

TABLE 3.4: Cash Flow for Solar Arrays 1 and 2

Year	Solar Array 1 Savings($)	Solar Array 2 Savings ($)
1	151	165
2	158	173
3	165	181
4	173	189
5	181	198
6	189	207
7	198	217
8	207	227
9	217	238
10	227	249
11	238	261
12	249	273
13	261	286
14	273	299
15	286	313
16	299	327
17	313	343
18	328	359
19	343	376
20	359	393
21	376	411
22	393	431
23	412	451
24	431	472
25	451	494
26	472	517
27	494	541
28	517	567
29	542	593
30	567	621

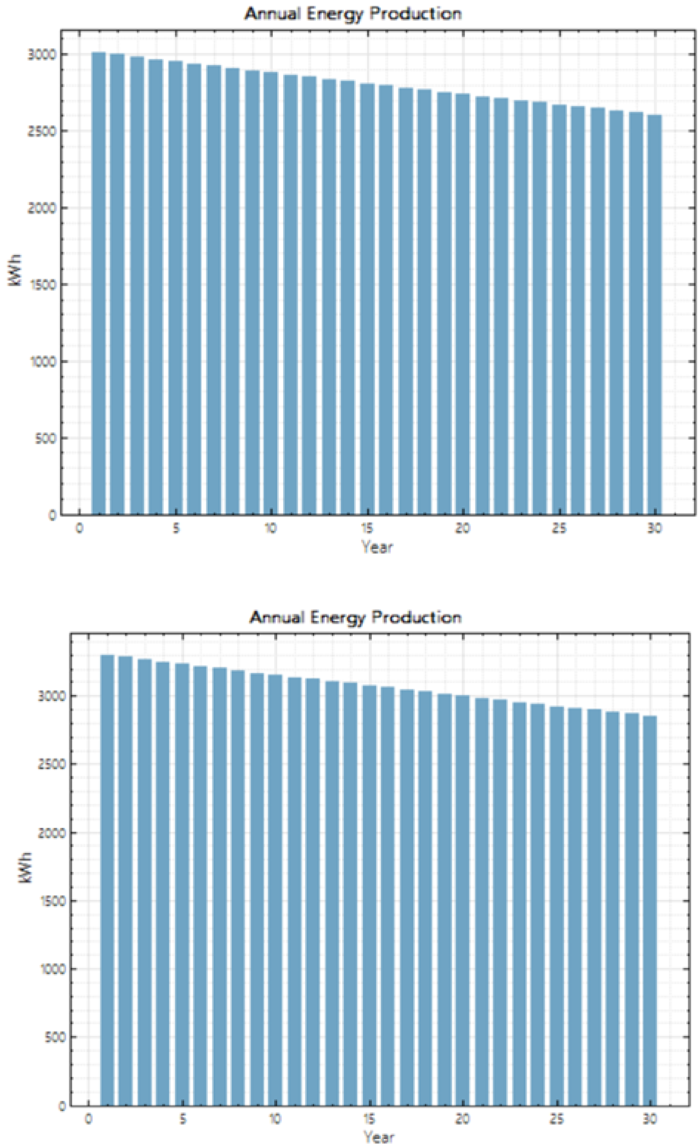

FIGURE 3.3: Annual Energy Production for Solar Array 1(top) and 2(bottom).

arrays. It can be concluded that the project was over designed for the load, cause the electricity production is very higher than the required to meet the system load, so it would be possible to run a lot of vehicles at the same time using the solar systems designed.

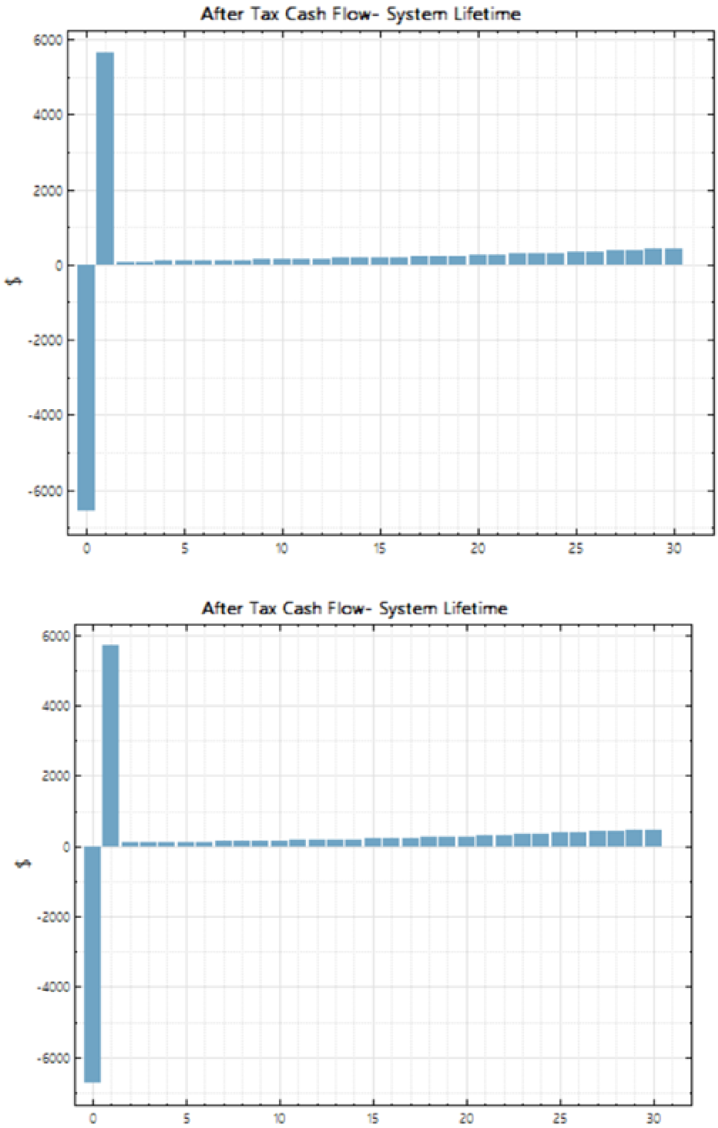

FIGURE 3.4: After Tax Cash Flow for Solar Array 1(top) and 2(bottom).

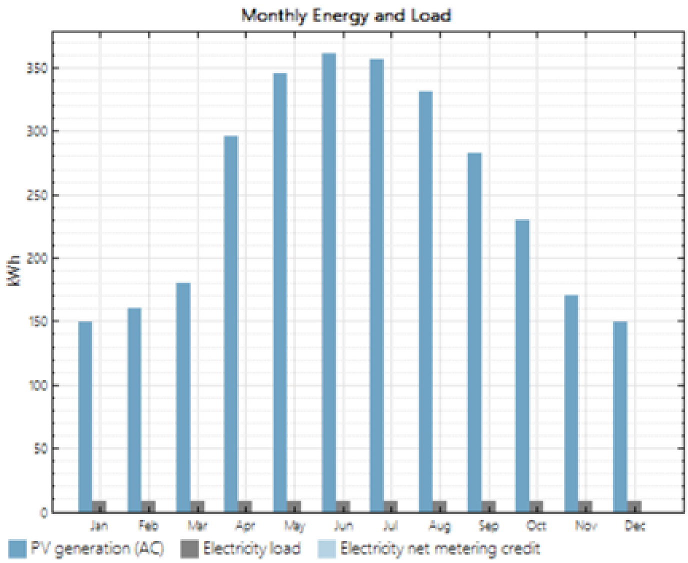

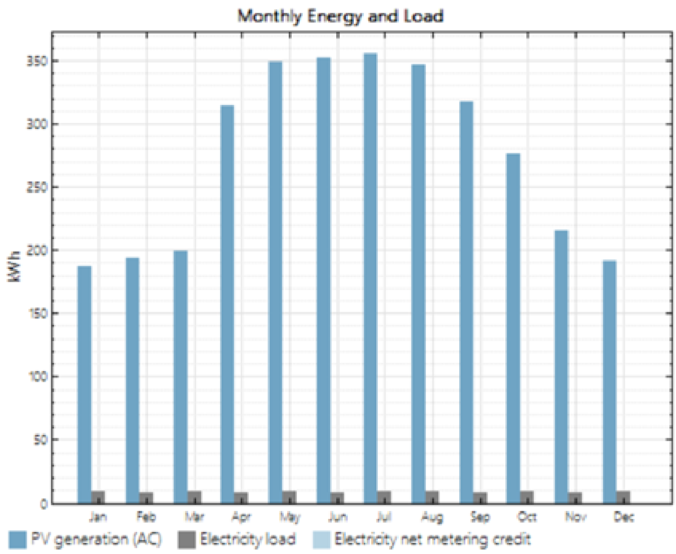

FIGURE 3.5: Monthly Energy and Load for Solar Arrays 1(top) and 2(bottom).

4 Conclusion

The comparison between the two analysis shows that the solar array 2 is the best choice for the solar energy conversion system to be installed on the full scale model, because of the better financial and performance parameters, even though solar array 2 has higher initial costs. One of the possible reasons for this conclusion is that, in solar array 2, all the modules are facing south, which is the best performance option for solar system in the North Hemisphere, and solar array 1 has 4 panels facing North. Also, Solar array 2 has less modules than the other one which decreases possible losses in the subarrays by various reasons, like wiring, mismatch, nameplate, etc, and modules FLEX-02W have higher efficiency then modules FLEX-02N. It would be possible to put solar array 1 in a North-South disposition, but this would decrease the 12-panel subarray performance to increase the 4-panel subarray performance, which would decrease the overall energy production. It can be observed that monthly energy production is higher in months of the middle of the year, which is expected because this is summer in North hemisphere.

The analysis that was made possible by SAM shows how useful this software can be to design energy systems, and there are lots of engineering applications for projects made by this software. Making this project added knowledge about how photovoltaic systems are designed, what are the important parameters for it, and which variables have to be considered when it is necessary to decide if it is feasible to install a photovoltaic energy system or not. The simulations made were models of the solar systems, but to install real systems, more considerations would have to be made, like ambient contracts and requisites to be attended, for instance. SAM offers a lot more information about the designed systems that the showed in this work, so it is possible to make deeper analysis to evaluate the feasibility of a given solar energy conversion system.

Bibliography

BIKANERIA SURYA PRAKASH JOSHI, A. J. J. Modeling and simulation of pv cell using one-diode model. **International Journal of Scientific and Research Publications**, v. 3, n. 2250-3153, p. 4, out. 2013. Disponível em: <http://www.ijsrp.org/research-paper-1013/ijsrp-p2249.pdf>. Acesso em: 15 aug. 2015.

BUSINESS Investment Tax Credit (ITC): Last updated may 13,2015. 2015. Disponível em: <http://programs.dsireusa.org/system/program/detail/658>. Acesso em: 18 aug. 2015.

CALIFORNIA Property Taxes 2015: California property taxes. 2015. Disponível em: <http://www.tax-rates.org/california/property-tax>. Acesso em: 20 sep. 2015.

EUROPEAN or CEC Efficiency: Grid inverters. 2014. Disponível em: <http://files.pvsyst.com/help/inverter_euroeff.htm>. Acesso em: 03 nov. 2015.

FADIGAS, E. A. F. A. Energia solar fotovoltaica. In: GRUPO DE ENERGIA ESCOLA POLITÉCNICA DE SÃO PAULO. **Fundamentos, Conversão e viabilidade técnico-econômica**. São Paulo, 2000. p. 90 – 92.

FEDERAL Tax Brackets: moneychimp. 2015. Disponível em: <http://www.moneychimp.com/features/tax_brackets.htm>. Acesso em: 05 nov. 2015.

GOSWAMI, D. Y.; KREITH, F.; KREIDER, J. F. **Principles of Solar Engineering**. 2nd. ed. Philadelphia: Francis & Taylor, 2000.

KING SIGIFREDO GONZALES, G. M. G. W. F. B. D. L. **Performance Model for Grid-Connected Photovoltaic Inverters**: Sandia report. Albuquerque, New Mexico and Livemore, California, 2007. Disponível em: <http://prod.sandia.gov/techlib/access-control.cgi/2007/075036.pdf>. Acesso em: 11 aug. 2015.

LEE, K. S. **Product Specification**: Recheargeable lithium ion battery - model: Icr18650 b3 2600mah. Seoul, 2010. Disponível em: <http://lib.store.yahoo.net/lib/theshorelinemarket/LG-18650-2600.pdf>. Acesso em: 14 nov. 2015.

MASTERS, G. M. **Renewable and Efficient Electric Power Systems**. 2nd. ed. [S.l.]: John Wiley & Sons, 2013.

MAUTHNER WERNER WEISS, M. S.-D. F. **Solar Heat Worldwide**: Markets and contribution to the energy supply 2013. Gleisdorf, Austria, 2015. Disponível em: <http://www.iea-shc.org/data/sites/1/publications/Solar-Heat-Worldwide-2015.pdf>. Acesso em: 15 oct. 2015.

NATIONAL Renewable Energy Laboratory: System advisor model (sam). 2015. Disponível em: <https://sam.nrel.gov/>. Acesso em: 05 nov. 2015.

OPTIMUM Tilt of Solar Panels. 2015. Disponível em: <http://solarpaneltilt.com/>. Acesso em: 03 jul. 2015.

ORDONEZ S. YANG, C. O.-J. O. J. V. T. S. M. B. E. C. J. Thermal simulation of an off-grid zero emissionns building. In: FLORIDA STATE UNIVERSITY, ES2014., 2014, Boston. **Proceedings of the ASME 2014 8th Internation Conference on Energy Sustainability**. Tallahassee: ASME, 2014. p. 7.

PROPERTY Tax Exclusion for Solar Energy Systems: Last updated november 6,2014. 2014. Disponível em: <http://programs.dsireusa.org/system/program/detail/558>. Acesso em: 17 aug. 2015.

SOLSTÍCIO energia: Mercado fotovoltaico. 2013. Disponível em: <http://www.solsticioenergia.com.br/sobre-energia-solar/mercado-fotovoltaico/>. Acesso em: 10 sep. 2015.

SPEER MICHAEL MENDELSOHN, K. C. B. **Insuring Solar Photovoltaics**: Challenges and possible solutions. California, 2010. Disponível em: <http://www.nrel.gov/docs/fy10osti/46932.pdf>. Acesso em: 12 aug. 2015.

TEAM, M. **Miasolé FLEX SERIES-02N**: Cigs flexible modules: High power density in a flexible form factor. Santa Clara County, California, 2015. Disponível em: <http://miasole.com/wp-content/uploads/2015/08/FLEX-02N_Datasheet_1.pdf>. Acesso em: 02 aug. 2015.

TEAM, M. **Miasolé FLEX SERIES-02W**: Cigs flexible modules: High power density in a flexible form factor. Santa Clara County, California, 2015. Disponível em: <http://miasole.com/wp-content/uploads/2015/08/FLEX-02W_Datasheet_1.pdf>. Acesso em: 02 aug. 2015.

TEAM, S. S. P. Spartan superway - annual report 2013. In: SAN JOSE STATE UNIVERSITY. **Spartan Superway Project - Annual Report 2013**. San Jose, California, 2013. p. 280 – 287.

TEAM, S. S. P. Spartan superway - annual report 2015. In: SAN JOSE STATE UNIVERSITY. **Spartan Superway Project - Annual Report 2015**. San Jose, California, 2015. p. 160 – 163.

U.S DEPARTMENT OF ENERGY. The hystory of solar. In: . California, 2002. p. 10 – 12.

FOLHA DE REGISTRO DO DOCUMENTO			
1. CLASSIFICAÇÃO/TIPO TC	2. DATA 17 de novembro de 2015	3. DOCUMENTO Nº DCTA/ITA/TC-031/2015	4. Nº DE PÁGINAS 85
5. TÍTULO E SUBTÍTULO: Performance and Financial Analysis of Solar Photovoltaic Systems			
6. AUTOR(ES): **Élvis Falcão de Araújo**			
7. INSTITUIÇÃO(ÕES)/ÓRGÃO(S) INTERNO(S)/DIVISÃO(ÕES): Instituto Tecnológico de Aeronáutica – Divisão de Engenharia Mecânica – ITA/IEM			
8. PALAVRAS-CHAVE SUGERIDAS PELO AUTOR: Costs; Energy; Photovoltaics			
9. PALAVRAS-CHAVE RESULTANTES DE INDEXAÇÃO: Efeito fotovoltaico; Conversão de energia; Fontes alternativas de energia; Custos; Radiação Solar; Engenharia elétrica.			
10. APRESENTAÇÃO: **(X) Nacional** ( ) **Internacional** ITA, São José dos Campos. Curso de Graduação em Engenharia Mecânica Aeronáutica. Orientador: Prof. João Batista do Porto Neves Júnior. Defesa em 18/11/2015. Publicado em 2015.			
11. RESUMO: This work is an performance and financial analysis of different designs for photovoltaic solar panel arrays to be installed in an Automated Transit Network Prototype with the objective of supplying the necessary electricity to make it work properly. An Automated Transit Network is a personal transportation system that moves following guideways and works automatically, with no driver, going directly to the station chosen by the rider without stop. The prototype is a project of San Jose State University called Spartan Superway and consists of a suspended cabin moving under a guideway.The designed systems would be installed above the tracks. An electrical photovoltaic system is consisted of solar modules arrays connected in parallel or in series attached to a Maximum Power Point Tracker that controls the operation point (voltage and current) to optimize power output. This is linked to a DC load, or a battery, or an inverter that produces AC power to be input into an AC Load or into the grid. The analysis for each design considered data about the local weather to calculate annual irradiance, wind speed and temperature, performance characteristics of modules and inverters used in the system, possible losses caused by shading, snow, mismatch, diodes and connections, DC wiring, nameplate, DC optimizer, AC wiring or step-up transformer, lifetime degradation, battery configurations, system costs, financial parameters, federal and state incentives, electricity rates and electric load. The results include a monthly evaluation of cash flow and energy production and a list of financial and performance parameters of the photovoltaic systems.			
12. GRAU DE SIGILO: **(X) OSTENSIVO** ( ) **RESERVADO** ( ) **CONFIDENCIAL** ( ) **SECRETO**			